

EFFECT OF THREE DIMENSIONAL FORCING ON THE WAKE OF A CIRCULAR CYLINDER

Except where reference is made to the work of others, the work described in this thesis is my own or was done in collaboration with my advisory committee. This thesis does not include proprietary or classified information.

Samik Bhattacharya

Certificate of Approval:

Roy Hartfield
Professor
Aerospace Engineering

Anwar Ahmed, Chair
Associate Professor
Aerospace Engineering

J Khodadadi
Professor
Mechanical Engineering

George Flowers
Dean
Graduate School

EFFECT OF THREE DIMENSIONAL FORCING ON THE WAKE OF A CIRCULAR CYLINDER

Samik Bhattacharya

A Thesis

Submitted to

the Graduate Faculty of

Auburn University

in Partial Fulfillment of the

Requirements for the

Degree of

Master of Science

Auburn, Alabama
August 10, 2009

EFFECT OF THREE DIMENSIONAL FORCING ON THE WAKE OF A CIRCULAR CYLINDER

Samik Bhattacharya

Permission is granted to Auburn University to make copies of this thesis at its discretion, upon the request of individuals or institutions and at their expense. The author reserves all publication rights.

Signature of Author

Date of Graduation

VITA

Samik Bhattacharya, son of Mr. Jayanta Bhattacharya and Mrs. Sila Bhattacharya, was born on 3rd November, 1983 in Kolkata, India. He received his bachelor's degree in Mechanical Engineering in 2005 from National Institute of Technology, Warangal, India. After his undergraduate degree, he worked as a junior scientist in DRDL, India. In 2007 he joined the Aerospace Engineering Department of Auburn University, USA. The research work presented here is the thesis done for the requirement of master's degree.

THESIS ABSTRACT

EFFECT OF THREE DIMENSIONAL FORCING ON THE WAKE OF A CIRCULAR CYLINDER

Samik Bhattacharya

Master of Science, August 10,2009

(B.Tech., National Institute of Technology,Warangal,India,2005)

75 Typed Pages

Directed by Anwar Ahmed

The periodic wake of a circular cylinder was investigated with a three dimensional disturbances,introduced in the flow field through two sinusoidal slits located on two diametrically opposite direction on the cylinder surface. Two speakers were used for periodic forcing. Experiments were conducted at Reynolds number of 24,000 and 45,000. It was found that an excitation frequency which was twice the shedding frequency was able to eliminate the shedding peak. At lower Reynolds number the drag measurement showed that maximum drag reduction was achieved when the excitation frequency was almost four times the natural shedding frequency. The basic mechanism of cancellation of shedding peak was found to be linked to the introduction of three dimensional disturbance which disrupted the formation of Karmann vortex street. This resulted in a distribution of energy from the shedding peak to smaller scales. The introduction of three dimensional disturbance accelerated the separating shear layers which narrowed the wake and made it uniform in terms of mean velocity.

ACKNOWLEDGMENTS

I would like to thank the Department of Aerospace Engineering of Auburn University for giving me an excellent opportunity to complete my master's degree and to utilise the experimental facilities. I am grateful to Mr. Andrew Weldon for his help with the fabrication of experimental set-up. I would also like to thank Dr. Roy Hartfield and Dr. J. Khodadadi for kindly consenting to be in my thesis committee. Mere acknowledgment or saying thank you to my advisor, Dr. Anwar Ahmed will not ever be sufficient to describe my gratitude for all that he has done for me, so I restrain from doing that mistake.

Style manual or journal used Journal of Approximation Theory (together with the style known as “aums”). Bibliography follows van Leunen’s *A Handbook for Scholars*.

Computer software used The document preparation package T_EX (specifically L^AT_EX) together with the departmental style-file `aums.sty`.

TABLE OF CONTENTS

LIST OF FIGURES	x
1 INTRODUCTION	1
1.1 Bluff body flow:	1
1.2 Need for control:	3
1.3 Classification of control methods:	4
1.4 Passive control:	4
1.4.1 Modification of body geometry:	4
1.4.2 Surface modification:	5
1.5 Active flow control:	6
1.6 Effect of sound on the flow over a circular cylinder:	8
1.7 Present research:	10
2 EXPERIMENTAL SETUP	12
2.1 The wind tunnel:	12
2.2 Cylinder models:	13
2.3 Instrumentation:	13
2.3.1 Data acquisition system:	13
2.3.2 Pressure measurements:	14
2.3.3 Hot wires:	14
2.3.4 Probe traversing system:	15
2.3.5 Speakers:	16
3 RESULTS AND DISCUSSION	18
3.1 Effect of excitation on the vortex shedding:	18
3.2 Effect of excitation on mean velocity distribution:	21
3.3 Effect of excitation on fluctuating quantities:	23
3.4 Characteristics of the flow field:	32
3.5 Kinetic energy in the wake:	33
3.6 Wake preservation:	33
3.7 Wake formation length:	38
4 CONCLUSION	52
BIBLIOGRAPHY	53
APPENDICES	56

A	CALIBRATION	57
A.1	Pressure transducer calibration:	57
A.2	Calibration of the hot wire:	59
A.2.1	Determination of two component of velocity from X-wire:	59
B	UNCERTAINTY ANALYSIS	63
B.1	Velocity sample uncertainty:	64
B.2	Sample calculation of pressure transducer calibration uncertainty:	64

LIST OF FIGURES

2.1	Schematic of experimental setup in the wind tunnel	17
2.2	Location of the sinusoidal slits on the cylinder surface	17
3.1	Energy spectra for different forcing frequencies	22
3.2	Cross sectional distribution of mean velocity, $Re=24,000$	24
3.3	Cross sectional distribution of mean velocity, $Re=45,000$	25
3.4	Half wake width	26
3.5	Variation of half wake width	27
3.6	Cross sectional distribution of velocity fluctuation v' , $Re=24,000$	28
3.7	Cross sectional distribution of velocity fluctuation v' , $Re=45,000$	29
3.8	Cross sectional distribution of velocity fluctuation u' , $Re=24,000$	30
3.9	Cross sectional distribution of velocity fluctuation u' , $Re=45,000$	31
3.10	Contour plot of the magnitude of the shedding peak, $Re=24,000$	34
3.11	Contour plot of the magnitude of the shedding peak, $Re=45,000$	35
3.12	Cross sectional distribution of turbulent kinetic energy, $Re=24,000$	36
3.13	Cross sectional distribution of turbulent kinetic energy, $Re=45,000$	37
3.14	Similarity parameter in wake, $Re=24,000$	39
3.15	Similarity parameter in wake, $Re=24,000$	40
3.16	Similarity parameter in wake, $Re=24,000$	41
3.17	Similarity parameter in wake, $Re=45,000$	42
3.18	Similarity parameter in wake, $Re=45,000$	43

3.19	Similarity parameter in wake,Re=45,000	44
3.20	Wake formation length,Re=24,000	46
3.21	Wake formation length,Re=24,000	47
3.22	Wake formation length,Re=24,000	48
3.23	Wake formation length,Re=45,000	49
3.24	Wake formation length,Re=45,000	50
3.25	Wake formation length,Re=45,000	51
A.1	Calibration curve for pressure transducer	58
A.2	Calibration curve for single wire	60
A.3	Calibration curve for x wire	61

CHAPTER 1
INTRODUCTION

1.1 Bluff body flow:

The flow over a bluff body has been the topic of extensive investigation over the years both due to its practical application and also because of the interesting fluid dynamic characteristics. Detailed review of this subject has been done by Berger and Wille [1], Bearman [2], Oertel [3] and Williamson [4]. Various features of this flow have been explored by investigating the flow over a circular cylinder which is regarded as a canonical bluff body flow. In spite of a simple geometry, the flow over a cylinder contains a rich diversity in behaviour as interaction of different shear layers, existence of certain instabilities (of which the most predominant is Von Karmann shedding), periodicity in flow etc. Apart from these the Reynolds number dependence, response of the flow to perturbation, the resultant drag and lift force acting on the body, have been the topic of extensive research. The flow over a circular cylinder is also a benchmark case of wake turbulence. The distribution of different turbulent quantities in the wake, the existence of turbulence structures of different length scales and their mutual interaction in terms of energy distribution have been investigated by several researchers [5],[6],[7]. Lately the introduction of concepts of non linear systems have enabled the researchers to interpret the different aspects of transition, turbulence and the flow structures in the light of non linear instability, bifurcation etc. However among the vast pool of research activities so far, the most prominent candidate which has caught attention of many researchers is Karmann shedding which is periodic shedding of vortex street from both sides of the cylinder. This is unique feature of bluff body flow which starts off after a certain Reynolds number is reached and has a definite frequency which is expressed in non

dimensional form as Strouhal number. Vortex shedding has been identified as a primary instability of the flow which is considered to be an inviscid phenomenon.

During shedding the flow behaves as a non linear oscillator where the controlling parameter is the Reynolds number. As the Reynolds number is increased the flow over a cylinder starts to bifurcate to higher periodicity and gradually it attains the turbulent stage. The frequency of shedding is very important from practical point of view since once it coincides with the natural frequency of the bluff body, gives rise to large fluctuating forces due to resonance causing structural vibration which eventually leads to catastrophic structural failure of the body. This phenomenon is famously known as vortex induced vibration. ([8],[9],[10],[11],[12],[13],[14]).

Another critical aspect of bluff body flow is flow separation. The boundary layer formed on the surface of the cylinder can not overcome the adverse pressure gradient and separates from the surface forming a free shear layer. This separated shear layer, at a certain Reynolds number becomes unstable via Kelvin Helmholtz instability. The shear layers roll up and form Helmholtz vortices which ride on the Karmann vortex street. After a certain Reynolds number the Karmann vortex street itself becomes wavy along the span and thus forms streamwise vortices. The root of the streamwise vortex can be observed as a pair of mushroom shaped region[15]. The shear layers from both sides of the cylinder cross the center of the wake at a distance from the center of the cylinder which is known as the formation length. The formation length is also defined as the region where the outside fluid crosses the center for the first time due to entrainment. All of these factors contribute to the formation of low pressure region behind the cylinder which in turn gives rise to drag acting on the cylinder, and to the three dimensionality which causes turbulence at higher Reynolds number.

1.2 Need for control:

Flow control aims at controlling the different parameters of the flow over a bluff body to achieve desired flow characteristics. The primary goals of most of the flow control techniques can be classified as follows,

1. To suppress vortex shedding :

Control of vortex shedding is necessary to prevent vortex induced vibration. For offshore structures, oil rigs, bridges, it is very much important from the view point of structural integrity and safety.

2. To influence three dimensionality in the flow:

Increased three dimensionality in the wake of a body moving through a fluid, help to reduce drag. It is desired to have increased mixing in case of an application where transport of some scalar properties are involved (heat transfer application). In a gas turbine engine the fuel needs to be properly mixed by atomisation with the working fluid.

3. To suppress flow induced noise:

The source of noise in a high speed flow is the turbulent boundary layer. Flow induced noise is a major factor for hypersonic flights.

Controlling the location of boundary layer separation point is an important criteria in engineering applications. On an aircraft wing it is desired to delay the flow separation on the airfoil at a high angle of attack to prevent stall. In case of a pipe flow boundary layer separation accounts for the losses in total pressure. In a gas turbine engine, the efficiency of expansion in a nozzle suffers due to separation inside the nozzle. Transition Reynolds number signifies the limit of the flow speed after which the boundary layer becomes turbulent. Depending on the application it may be required to delay or advance transition. Turbulent boundary layer contains high momentum thus it is more effective in overcoming the adverse pressure gradient, thus separation gets delayed.

A review of flow control research has been done by Choi et al[16].

1.3 Classification of control methods:

Flow control methods can be classified into two groups.

- Passive control
- Active control.

1.4 Passive control:

In this control method passive devices are used to alter the flow features. Following are the examples of pasive control

1.4.1 Modification of body geometry:

By using a wavy cylinder Ahmed et al [17] found that behind the nodal points of attachment, a locally narrower wake developed and more rapid wake velocity recovery was observed compared to the saddle points of attachment. Tanner [18] investigated the effect of various forms of segmented trailing edge wings and measured drag reduction upto 64%. Bearman and Owen [19] achieved 30% drag reduction and suppression of vortex shedding at Reynolds number of 40,000 by using plates whose front face had spanwise sinusoidal variation. Rodriguez [20] used a three dimensional trailing edge consisting of alternate segments of blunt base and spanwise cavity as a drag reduction device. He found that an optimized shape of the configuration led to 40% drag reduction. Tombazis and Bearman[21] studied the effect of three dimensional geometric disturbance on the wake by using a blunt based body with a wavy trailing edge. They found that drag reduced due to increased base pressure, which in turn was a result of dislocation of karman vortex street. Park et al [22] used a bluff body with a blunt trailing edge and with small tab attached on the upper and lower trailing edges of the bluff body. The experiment was conducted at Re of 20,000,40,000

and 80,000. They found that for an optimum tab configuration the base pressure increased by 30%. The Karman shedding was also completely eliminated behind the bluff body.

All the above methods essentially introduced some kind of spanwise variation of the bluff body. Consequently spanwise phase mismatch occurred in the Karmann vortex street and the two dimensional nature of the vortex street was lost. The resulting three dimensionality disrupted the formation of Karmann vortex street in the near wake of the cylinder. Due to the increased three dimensionality, the base pressure increased resulting in less drag on the body.

1.4.2 Surface modification:

Lee and Kim [23] used cylinders with wires wrapped on them helically. As a result of this modified surface, the vortex formation region was elongated and the vortex shedding frequency decreased. The wake width narrowed due to disruption of large scale vortices. Flow around circular cylinder with U and V shaped grooved surfaces was investigated by Lee and Lim [24]. They found that U type grooves reduced the drag by 18.6% compared to the smooth cylinder whereas the drag reduction was only 2.5% for V type grooves. Lee et al [25] used a V grooved micro-riblet with a peak to peak spacing of 300 micrometers. At a cylinder Reynolds number of 3600 they achieved a maximum drag reduction of 7.6%. However they noted an increase in drag with increasing Reynolds number. Zhdanov and Papenfuss [26] investigated the effect of thin plates and dimples on the boundary layer to achieve base pressure variations and drag. The prototype bluff body was a bus-coach model. The use of plates and dimples decreased the Reynolds stress, mean velocity defect and the wake width was narrowed down. This was attributed to the formation of weaker and smaller vortices behind the model.

The above methods of flow control do not interfere with the wake directly. Most of them affect the boundary layer transition or separation point. On the other hand control can be made effective by directly modifying the wake. One such method is using splitter plates in the wake. Roshko [27] used a circular cylinder with a solid splitter plate (about

five cylinder diameters) attached to it. Due to the interference of the splitter plate the base pressure was substantially increased and the vortex formation was inhibited. Use of a smaller length splitter plate (1.1d) showed that when the leading edge of the splitter plate was located at downstream positions within about 2.5d, the base pressure and the shedding frequency was affected. But further downstream movement of the splitter plate was not effective to alter the base pressure and shedding frequency.

1.5 Active flow control:

Active flow control employs various forcing mechanisms to effect the flow over a bluff body. Fujisawa et al [28] studied the flow field of a rotationally oscillating cylinder. The strouhal number based on forcing frequency was 1. Their measurement showed substantial reduction in the fluctuating velocity at the optimum phase control. Due to the oscillation the large scale structure of vortex shedding was almost removed in the cylinder wake. Effect of stream wise oscillation of a circular cylinder on the wake was investigated by Cetiner and Rockwell [29]. Their result showed that for $\frac{f_e}{f_0}$ (where f_e =frequency of oscillation of the cylinder, f_0 =vortex shedding frequency) =1,0.44,0.74,0.88, they could achieve lock on stage which was evident in the spectra of transverse force coefficient. They also found that during one cycle of cylinder oscillation the vortex formation patterns were comprised of a Karmann like shedding and a nearly frozen array of shed vortices.

Tokamaru and Dimotakis [30] carried out experiments to study the effect of sinusoidal rotation of cylinder on the wake. The cylinder was rotated sinusoidally in time at a frequency f and a normalised peak rotation rate σ . The normalised peak rotation rate was chosen such that peak peripheral velocity was comparable to the velocity just outside the boundary layer. The strouhal number based on the forcing frequency was varied between 0.17 and 3.3. The plot of drag coefficient vs forcing strouhal number for a normalised peak rotation rate of 2 ,showed that the estimated C_d for the unforced case is a factor of six greater than the forced case.Also for certain forcing frequency the wake structure was synchronised with

the forcing frequency. They concluded that the dynamics of the wake was controlled by the ejection of circulation into the flow rather than the behaviour of the unforced flow.

In the study done by Kieft et al [31] a circular cylinder was heated and the corresponding effect on the vortex formation was found. The Reynolds number for the experiment was 75. Another important non dimensional number for this case is Richardson number which is defined as the ratio of buoyancy force and inertial force. The Richardson number was varied between 0 and 1. They found that the induced heat caused a downward motion for the shed vortex structure. This behaviour was attributed to the difference in strength between two vortex rows.

Another important method of active flow control is the use of synthetic jet. Glezer and Amitay [32] used a control device which was used to inject linear momentum to the flow. The synthetic jet is formed by alternating momentary injection and suction of fluids across an orifice. But since the working fluid is the ambient fluid the net mass flux is zero where there is a non zero momentum injection into the flow. They found that the high frequency synthetic jet over a circular cylinder caused a significant drag reduction. The accelerated cross flow around the jet orifice caused the stream wise pressure gradient to change such that the boundary layer downstream becomes thinner allowing the flow to overcome adverse pressure gradient and thus delaying flow separation.

A relatively new flow control method which has gained prominence in recent times is the use of plasma actuators. This term refers to a broad class of device based on atmospheric pressure electrical discharges and include corona discharges, dielectric barrier discharges (DBDs), glow discharges and arc discharges. In DBD plasma actuators two electrodes are separated by a dielectric material, one of them is left open to atmosphere whereas the other is embedded into the surface of the body. A DBD plasma is created when a high voltage is applied to the electrodes. The residual fluid is driven in the form of a horizontal jet by the induced velocity. This induced velocity is higher in the case of the application of glow discharge plasma where it has been shown that the higher induced velocity actually

caused addition of near wall flow momentum and as a result boundary layer separation was delayed [Roth et al [33]].

Prandtl first demonstrated the effect of boundary layer suction on the flow around a circular cylinder. When the slow flow in the boundary layer is removed by suction, the boundary layer gets energized by the rotational effect created by it. The same effect can be achieved by blowing [34]. The main advantage of boundary layer control is attached flow due to modified pressure gradient and delay of separation of the boundary layer.

Another active control method which directly interfere with the wake is base bleeding. Bearman [35] successfully used base bleeding to suppress vortex shedding and to reduce base drag. Like splitter plate the effect of base bleeding was to delay the interaction of the two separated shear layers and thus to increase the formation length. The base pressure increased due to an increase in vortex formation length.

1.6 Effect of sound on the flow over a circular cylinder:

In addition to the active techniques mentioned earlier some investigators have used acoustic disturbances to affect the bluff body wake. Blevins [36] investigated the influence of sound waves on the vortex shedding from a circular cylinder. The Reynolds number range for the experiment was 20,000-40,000. His results showed that application of sound correlated with the span wise vortex shedding. This was confirmed by the signals obtained from four flush film sensors placed on different span wise locations on the cylinder. In the absence of excitation the signals were incoherent and irregular. When 143.5 dB sound at the shedding frequency was introduced the four signals were nearly in phase with less irregularity which showed that application of acoustic excitation synchronized the shedding frequency and was able to increase the strength of vortex shedding. Another important finding from this experiment was that the sound applied near vortex shedding frequency shifted vortex shedding to the forcing frequency.

Detemple- Laake and Eckelmann [37] carried out detailed experiments to understand the coupling mechanism between vortex formation and shedding with sound waves. The

Reynolds numbers for the experiments were selected between 53 and 250. The ratio of frequency of the sound wave to the natural vortex shedding frequency of the cylinder (in the unforced case) was varied between 0.5 and 4. Depending on the sound frequency and the sound amplitude, twelve different wake structures were found. They were broadly classified as

- structures independent of the ratio of sound frequency to vortex shedding frequency.
- synchronised structure which was shedding frequency equal to half the sound frequency
- synchronised structures where the shedding frequency was same as the sound frequency.

Hsiao and Shyu [38] introduced acoustic waves in the cylinder wake through a thin slit on the cylinder surface. The results showed that the separated shear layers were sensitive to the excitation. When the frequency of the internal acoustic excitation was around the shear layer instability frequency the drag reduction was maximum and a marked reduction in the amplitude of the shedding frequency was observed. The flow visualization also showed that the Karman vortex street was perturbed to form smaller vortices that significantly increased the three dimensionality of the wake.

Huang [39], performed an experiment with circular cylinder in the Reynolds number range from 4,000-8,000 by introducing pure tone sound at the natural vortex shedding frequency into the flow through a thin slit on the cylinder surface. He found that vortex shedding was suppressed by the excitation but there was an optimum sound level for the maximum suppression. For a Reynolds number of 5,550, natural shedding frequency of 82 Hz and with a sound level of 70 db at the slit, the natural peaks were almost eliminated at $\frac{x}{d} > 7$. His results also showed that there was a very narrow excitation range which was able to suppress the shedding to the maximum. Out of these ranges the excitation had no effect on shedding.

Fujisawa et al.,[40] performed similar experiment with acoustic excitation. The cylinder diameter was 50 mm with an aspect ratio of 8. The flow velocity was 2 m/s resulting in a Reynolds number of 9,000. The drag coefficient calculated from the surface pressure distribution showed that it had a minimum for a slit angle of 90° , and when the excitation frequency was 4 times the natural shedding frequency i.e. around the unstable frequency of the shear layer.

In a similar study, Fujisawa et al.,[41]; investigated the effect of internal acoustic excitation with the help of phase averaged Particle Image Velocimetry(PIV). The Reynolds number of the experiment was 9,000. The phase averaged results showed the formation of discrete vortices along the shear layer of the cylinder wake when the excitation frequency was four times the vortex shedding frequency. Due to the interaction of the vortices with the wake the velocity fluctuation in the flow field was weakened.

1.7 Present research:

It may be noted that these studies with internal acoustic excitation have concentrated in the low Reynolds number range. The effect of internal acoustic excitation on cylinder wake at higher Reynolds number is still lacking in the literature. The flow over a cylinder at higher Reynolds number contains multiple global modes. Also at higher Reynolds number the amplitude of the global mode increases. Whether or not the internal acoustic excitation is successful in suppressing the shedding component which is the first global mode to become unstable and how exactly it influences the turbulent wake needs to be further investigated. Also all the research done so far, have used a straight slit which essentially introduce a two dimensional disturbance. By introducing a three dimensional disturbance through a wavy slit, is likely to be more effective. This is the motivation of the work presented in this thesis.

The objective of this research was to investigate the influence of three dimensional disturbance created by internal acoustic excitation of different frequencies on the turbulent wake of a circular cylinder. It is to be noted that the excitation introduced in the flow in the aforesaid manner works like a synthetic jet. Since the working fluid source for the excitation

is the surrounding fluid(in this case, air inside the cylinder),no extra mass flow was added to the system, though momentum was added through the sinusoidal slits to the flow due to vibration of the speaker diaphragm. The modification of the flow over the cylinder occurred owing to the action of the jet on the cross flow over the cylinder.

CHAPTER 2

EXPERIMENTAL SETUP

Sinusoidal slits were made on the cylinder surface on diametrically opposite locations. Two loud speakers were used to generate sound at desired frequencies and amplitudes. Thus the wake was subjected to three dimensional forcing. All the investigations were carried out at two Reynolds numbers, 24,000 and 45,000. Hot wire anemometers were used for measuring the turbulent quantities of the wake and pitot tube was used for total pressure survey. The data collected from the experiments were analysed to understand in detail the exact mechanism by which this three dimensional disturbance affect the wake. The drag on the cylinder was calculated from the total pressure data. One of the aim of this research was to find whether a disturbance with a frequency higher than the shedding frequency is able to cancel the Karmann shedding. This was investigated with the help of a single wire placed in the shear layer of the cylinder.

2.1 The wind tunnel:

All experiments were performed in the Auburn University 3x4 ,close circuit,low turbulence subsonic wind tunnel. The tunnel has a contraction ratio of 5,test section with 1.5 meters long and cross section of 1mx1.1m. The floor is made of steel section to which the experimental setup was attached. The side walls and the roof of the test section is made up of plexi glass. The speed of the tunnel is controlled from a control pannel and the corresponding readings were noted from a pitot tube attached to a port in the test section.The non uniformity in the flow was found to be 1% and a free stream turbulence level of 0.5%. The cylinder model was placed at a height of 470 mm from the wind tunnel

floor to minimize the effect of boundary layer developed on the ceiling and the floor of the wind tunnel. The test section blockage ratio was 0.045.

To mount the cylinder model in the center of the tunnel, a steel frame was used (see Figure 2.1). Two elliptic side plate were attached to both end of the cylinder to ensure two dimensional flow. Separate fixtures were fabricated from plywood plates for holding the speakers.

2.2 Cylinder models:

Cylinders were made of copper tubings of 41.3 mm outer diameter and thickness 1 mm. The length of the cylinders were 203 mm. So the aspect ratio of the cylinder was 4.9. Sinosoidal slits were made on two diametrically opposite location of the cylinder by laser cutting operation[see Figure 2.2]. The width of the sinosoidal slit was 0.5 mm and the length of the slit was 60mm.

2.3 Instrumentation:

2.3.1 Data acquisition system:

All data from the hot wires and pressure sensors used in this study were recorded using a data acquisition board (National Instrument NI PCI 6035E DAQ board). The A/D converter has 16 bit resolution over an bipolar input range of ± 10 volts. The maximum sampling rate of the A/D board is 200 kHz and it can handle 16 single-ended or eight differential analog inputs. All the data acquisition was done by using LabVIEW 8.2 software. Separate LabVIEW codes were written for data acquisition, signal generation and probe calibration. All the connections were made in a patch board outside, which was connected to the A/D board in the CPU of the computer. Proper care was taken to insulate the connection from outside interference which introduce noise.

2.3.2 Pressure measurements:

Total pressure in the wake was measured by using pitot tube. The probe was mounted in the traverse system placed on the top plexglass roof of the wind tunnel, and was introduced in the test section through the slot. Care was taken to maintain the probe alignment perpendicular to the flow. The pitot probe was connected to a differential type pressure transducer (Validyne, model DP 45-14). It is a variable reluctance type transducer which gives the difference of the pressure from its two input connection. The other input tube was left open to the atmosphere. Breather between the test section and the diffuser in the return leg ensures the static pressure to be atmospheric. A carrier demodulator (Validyne, model CD 12) was used to provide transducer excitation and to amplify and demodulate the output signal of variable reluctance transducer. The input sensitivity of the carrier demodulator is 0.9-75 m V/V for 10 v dc full scale output. The output signal from the signal conditioner was sampled using the DAQ board.

2.3.3 Hot wires:

The turbulent quantities in the wake were measured with the help of hot wires. Hot wire measurements were performed using single wires (DANTEC P15) and x-wires (DANTEC 55P61). A constant temperature anemometer system (DANTEC MiniCTA) was used for this purpose. The overheat ratio of the hot wires was adjusted according to the manufacturer's prescribed maximum wire temperature. The total resistance was calculated by adding

1. the resistance of the cable and the probe holder together (while the probe holder was shorted using a shorting probe).
2. the resistance of the hot wire probe.

Resistance measurement was done with a voltmeter. The overheat ratio was calculated thereafter and the dip-switches were adjusted according to the calculation. The frequency

response of the hot wire circuitry and the gain settings were maintained at the manufacturer's specifications. The wire of the single sensor probe was made of platinum plated tungsten with a diameter of 5 micrometer and length 1.25 mm. According to manufacturer's specification the maximum sensor temperature permitted is $300^{\circ}C$. But during the experiments a wire temperature of $150^{\circ}C$ was selected to assure safe operation and longevity of the wire. The x wires had the same wire diameter and length as the single wire. It was too made of platinum plated tungsten. The angle between the two wires was 90° . The x wire was mounted with the probe axis parallel to the flow direction. So the angle between the mean flow direction and the wire was 45° . The signal from the anemometer was constantly monitored in a HITACHI oscilloscope. Like pressure measurements, the hot wire signal were sampled in the same manner using the DAQ board. The probe holder was fixed to a steel bar and mounted on the traverse. The anemometer was connected to the patch board in a differential mode since the MiniCTA anemometer did not have any in built ground reference (floating signal source).

2.3.4 Probe traversing system:

Probe access to the tunnel interior was provided by slots cut through the plexiglass plate at the top of the wind tunnel test section. The probe movement was controlled by a two axis traverse controller (VelMax). The traverse controller was connected to the personal computer through serial ports. Desired movement of the traverse were programmed by using the serial port commands, as mentioned in the manufacturer's manual, in LabVIEW software. The mounting rod end which housed the hot wire probe was made streamlined shape. The mounting rod was wrapped with duct tape to ensure smooth movement during the experiment. The vibration of the probe support was not significant as was checked from the various power spectrums.

2.3.5 Speakers:

Excitation to the flow was provided by two sub woofers. Two set of sub woofers were used for this purpose (PYRAMID-WX-65X). The speakers were operated by means of sinusoidal signals of desired frequencies, generated by LabVIEW and amplified by an external power amplifier for driving the speakers. It was found that an optimum voltage of 5-7 volt was sufficient for driving the speakers. Higher voltage was found to be harmful for the speakers in the high frequency range.

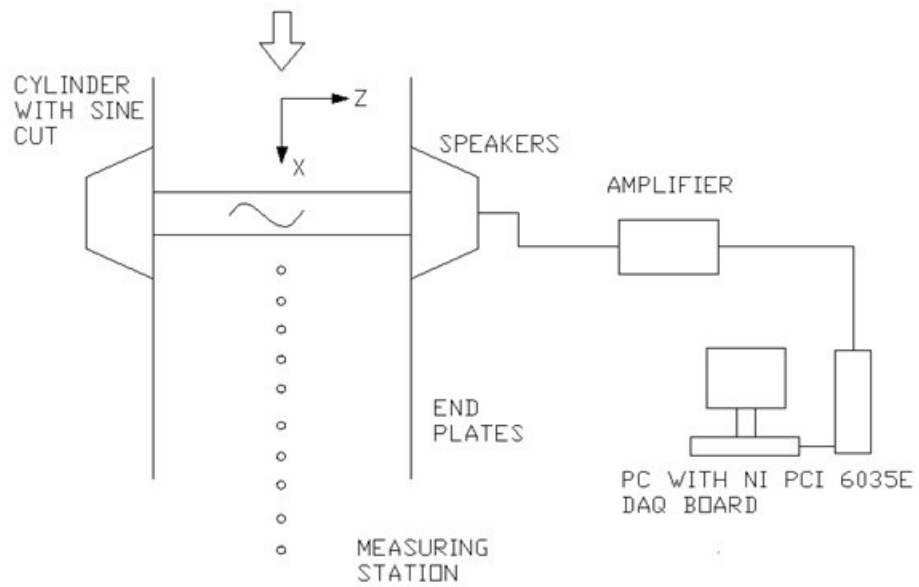


Figure 2.1: Schematic of experimental setup in the wind tunnel

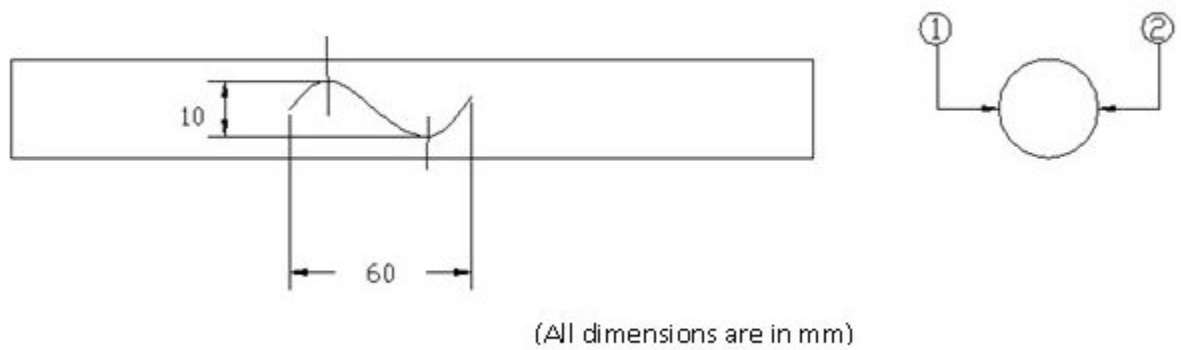


Figure 2.2: Location of the sinusoidal slits on the cylinder surface

CHAPTER 3

RESULTS AND DISCUSSION

The experiments were done at two different Reynolds numbers, 24,000 and 45,000, which correspond to 9 m/sec and 17 m/sec of free stream velocity in the wind tunnel. The cylinder was placed in between the end plates in such a way so that the mean axis of the sinusoidal slit on the top surface was at 90 degree from the attachment line. The blowing coefficient C_μ for each case was calculated as $C_\mu = \frac{v_s}{U_\infty}$, where v_s is the velocity of excitation from the slot. This was measured by placing the single wire very close to the slot. The wake measurements without acoustic excitation were accomplished with a solid cylinder model. Table 3.1 shows the various blowing coefficient values.

3.1 Effect of excitation on the vortex shedding:

A single wire was placed in the upper shear layer zone, $\frac{y}{d} = 0.5$ and $\frac{x}{d} = 1$, to measure the vortex shedding frequency f_{s0} . It was found to be 50 Hz for Re of 24,000. For Re of 45,000, this was found to be around 78 Hz. The speaker was operated with a number of different frequencies for the two Reynolds number case; the maximum being 180 Hz. It was not feasible to operate the speaker at higher frequencies since at higher ranges the amplitude

<i>Re = 24000</i>		<i>Re = 45000</i>	
Excitation Frequency (<i>Hz</i>)	C_μ	Excitation Frequency (<i>Hz</i>)	C_μ
25	0.2263	38	0.1284
45	0.2213	76	0.1266
50	0.2183	85	0.1237
60	0.2202	100	0.1217
100	0.2086	156	0.1252
180	0.2256	180	0.1278

Table 3.1: Blowing coefficients for different forcing frequencies

of the forcing goes down drastically making the forcing ineffective. For this reason in the higher Reynolds number case the frequency of 310 Hz ($4f_{s0}$) was not selected as it was found that at this frequency the blowing coefficient is not sufficient for the experiment.

Figure 3.1 shows the power spectrum plotted for different forcing frequencies. It is evident that for Re of 24,000 case when the frequency of the acoustic excitation was almost same as the natural shedding frequency the peak of the shedding component in the spectrum plot shifted towards the forcing frequency side with a nominal decrease in the magnitude of the component as seen from figure 3.1. This trend of nominal shift in frequency and reduction in magnitude continued for forcing frequency of 45 Hz. However there was a remarkable decrease in the peak when the forcing frequency was 60 Hz. The shedding peak was almost eliminated at this forcing frequency. This trend remained same for a forcing frequency of 100 Hz and 180 Hz. Lastly in the event of excitation with a sub harmonic frequency of 25 Hz (around $\frac{f_{s0}}{2}$) the only difference in the power spectra is the appearance of a distinct peak in the sub harmonic range of the spectrum with slight increase in the shedding component.

For Re of 45,000 case, the power spectrum shows that in the event of excitation with a frequency almost equal to the shedding frequency the shedding peak was considerably strengthened. When the forcing frequency was 85 Hz a distinct peak appeared around 176 Hz. In case of excitation with 100 Hz the peak shifted to 100 Hz and the shedding peak disappeared. The shedding peak was completely eliminated when higher excitation frequency of 156 Hz and 180 Hz was applied.

From the spectrum plots discussed so far it is clear that when the forcing frequency is twice the shedding frequency the acoustic excitation successfully eliminated the shedding peak completely. Except Huang's work (Huang X.Y, 1995) where he reported to have eliminated the shedding peak with a acoustic excitation of same frequency at a downstream distance greater than $\frac{x}{d} = 7$, all the other research done with internal acoustic excitation have shown that in the low Reynolds number range, a forcing frequency which is around four times the shedding frequency was necessary to neutralize the vortex shedding completely.

Hsiao et al (1991) did their experiment with a 6cm outer diameter cylinder and their result at Re of 24,000 (fig. 10 in the paper) showed that only when the forcing frequency was at least of the order one than vortex shedding frequency which was 18 Hz, excitation was able to eliminate the shedding . But in the present work, the shedding frequency was 50 Hz for Re of 24,000 case due to the use of a different diameter cylinder. Also the three dimensionality was introduced through a sinusoidal slit which invariably helps to increase the perturbation in the flow. So it is concluded that the main factor for cancellation of shedding is the degree of three dimensionality introduced which in turn depend on the slit geometry, blowing coefficient and the frequency of excitation. It is possible to achieve cancellation of shedding peak even with an excitation of frequency less than the shear layer instability frequency provided the blowing coefficient or in other words the amplitude of excitation is high and the resultant three dimensionality introduced is effective in disrupting the shedding pattern . This argument supports the flow visualization study done by Hsiao et al (1991) where it was shown that the basic mechanism for cancellation of shedding was the destruction of Karman vortices into smaller eddies near the cylinder.

The flow in the wake of a circular cylinder is a highly nonlinear phenomenon. It contains multiple modes of disturbances where the Karman vortex shedding is considered as the primary mode. When an external disturbance having almost the same frequency of the primary mode is introduced in the system which is in the form of an acoustic excitation in the present experiment, it can couple with the primary mode. The effect of coupling may either be to attenuate or amplify it depending on the phase difference of the two modes. The present work, as discussed in the previous paragraphs, showed weakening of shedding peak at Re of 24,000 and strengthening at Re of 45,000. This behavior of the spectral plot can be attributed to the inherent non linearity of the turbulent wake.

Regarding the use of the parameter which aptly describes the effectiveness of forcing, it is suggested that blowing coefficient is a better term to use than sound pressure level as used by previous researchers. The excitation created by the speaker diaphragm forces a jet out of the slit, into the flow. It is not the acoustics rather the amplitude and frequency

$Re = 24,000$		$Re = 45,000$	
Excitation Frequency (Hz)	C_d	Excitation Frequency (Hz)	C_d
No forcing	1.13	No forcing	1.20
50	1.08	76	1.02
180	0.56	180	0.84

Table 3.2: Drag coefficients for different forcing frequencies

of the jet which is important for effective shedding control. Furthermore acoustics depend not only on the signal input but also on the material used in model construction, internal cavity resonance due to standing waves etc.

3.2 Effect of excitation on mean velocity distribution:

Mean velocity profiles were measured by traversing an x wire sensor (DANTEC 55P15) in the wake starting from 1 diameter to 10 diameters downstream of the cylinder. The frequency for the acoustic excitation was maintained at fs_0 and 180 Hz. Figure 3.2 and figure 3.3 illustrate the effect of forcing with 180 Hz excitation on the mean velocity profiles in the two Reynolds number cases. Due to the forcing the upper and lower shear layers got accelerated. This acceleration of shear layers is evident in the presence of a large velocity gradient around the region $\frac{y}{d} = \pm 1$. This increase in velocity of the free shear layers effectively narrows down the wake thus making the region more uniform in terms of flow velocity. Apart from the clear indication of a narrowing wake, figure 3.2 and 3.3 also shows that up to about $\frac{x}{d} = 5$, the velocity of flow in the centerline of the wake has in fact came down in the case of forcing with 180 Hz excitation. This trend was not visible afterwards. From $\frac{x}{d} = 6$ to 10 the velocity profiles for the forcing case maintains the accelerating character of the shear layers and more uniform velocity profiles, thus indicating lower value of momentum loss from the no forcing case, which ultimately contribute to lower drag. The table 3.2 shows the C_d values computed from the velocity profiles.

It is interesting to note that at Re of 24,000, the drag reduction was almost 50% compared to 30% in case of Re of 45,000. To determine the effect of forcing on the evolution of the wake the half wake width was determined from the mean velocity profiles. The half

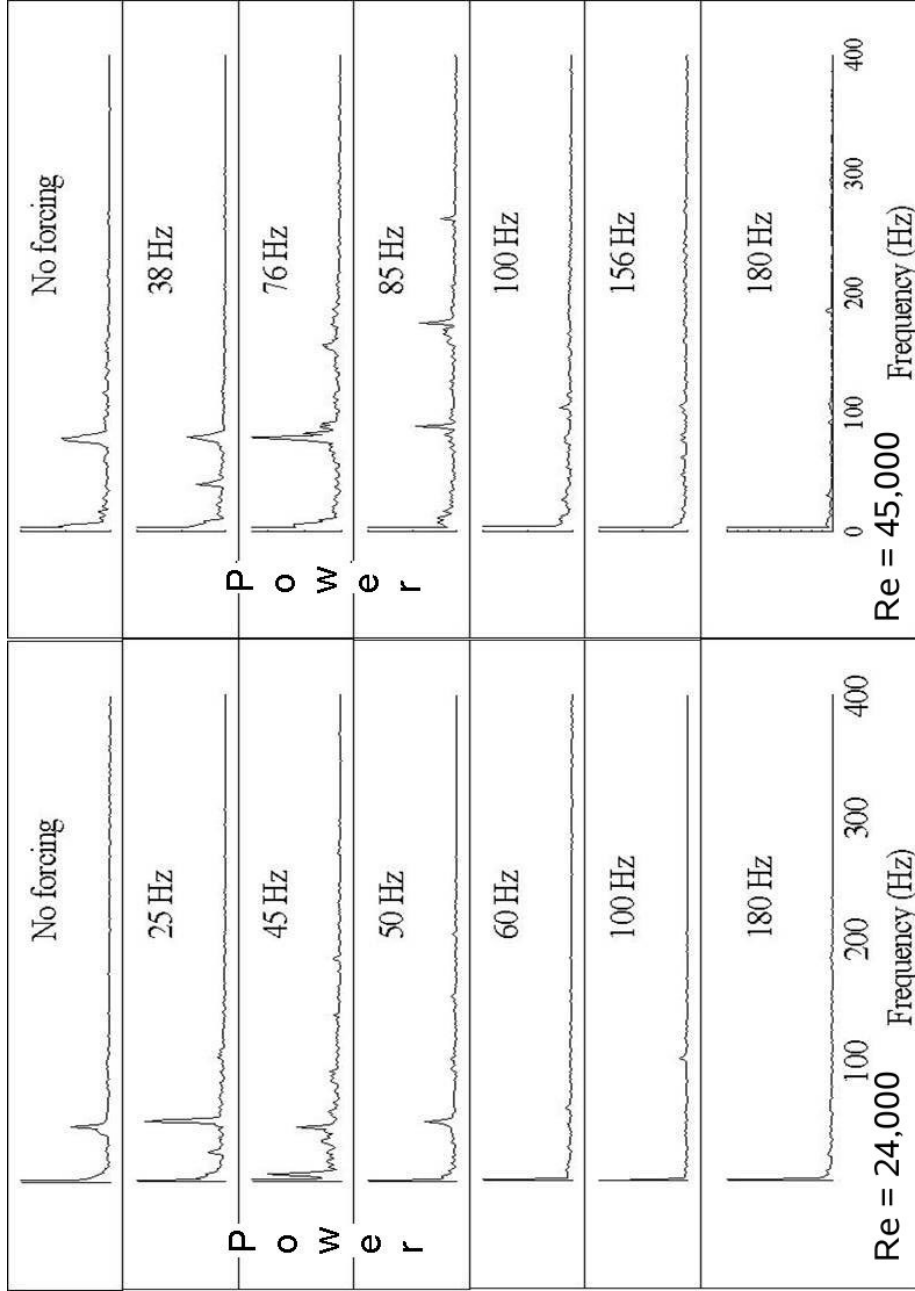


Figure 3.1: Energy spectra for different forcing frequencies

wake width δ is defined as the distance of the location from the center of the wake where the velocity defect is half the maximum velocity defect(see figure 3.4). From figure 3.5 it is evident that forcing caused the wake to narrow down in both the cases.

3.3 Effect of excitation on fluctuating quantities:

The cross sectional distribution of velocity fluctuation in the wake of the circular cylinder is shown in figure 3.6 to 3.9, where the results under acoustic forcing at 180 Hz have been compared with that of no forcing case. The normal and stream wise velocity fluctuations are mostly reduced by the application of forcing in lower Reynolds number case. This is attributed to the appearance of a more uniform wake in the case of forcing. In figure 3.6 and 3.7, around $\frac{y}{d} = 0.5, -0.5$ the v fluctuation increased primarily due to the three dimensionality introduced by the forcing which injects momentum into the flow. At all stream wise position the suppression of fluctuation is evident in case of 180 Hz forcing. However this suppression is not strong in the higher Reynolds number case as seen from the figure 3.7 and 3.9. Due to the high flow velocity in this case the magnitude of the forcing disturbance is not that effective in suppressing the velocity fluctuation compared to the low Reynolds number case. The suppression of the fluctuation can be related to the presence of stream wise vortices in the cylinder wake. Bays-Muchmore and Ahmed (1993) have shown that the creation of stream wise vortices depend on the dominant foci structure present along the secondary separation line. The peak values of turbulent shear stress and kinetic energy production occur where these stream wise vortices merge with the braids. So it may be assumed that forcing strongly affects the location of secondary separation line and consequently the production of the stream wise vortices which in turn results in less fluctuation. The assymetry in the distribution of the fluctuating quantities can be attributed to the high degree of disturbance in the very near wake of the cylinder.

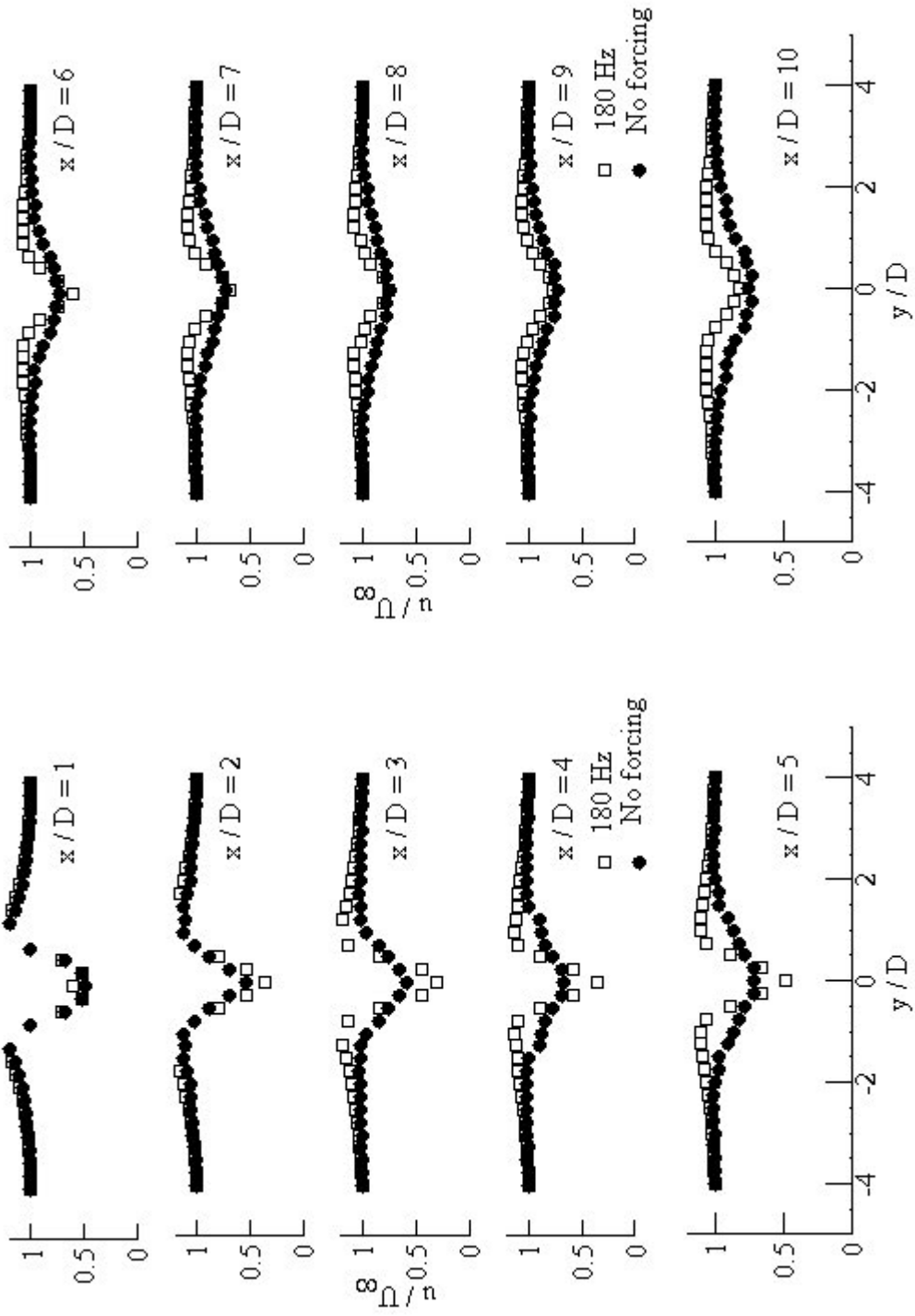


Figure 3.2: Cross sectional distribution of mean velocity, $Re=24,000$

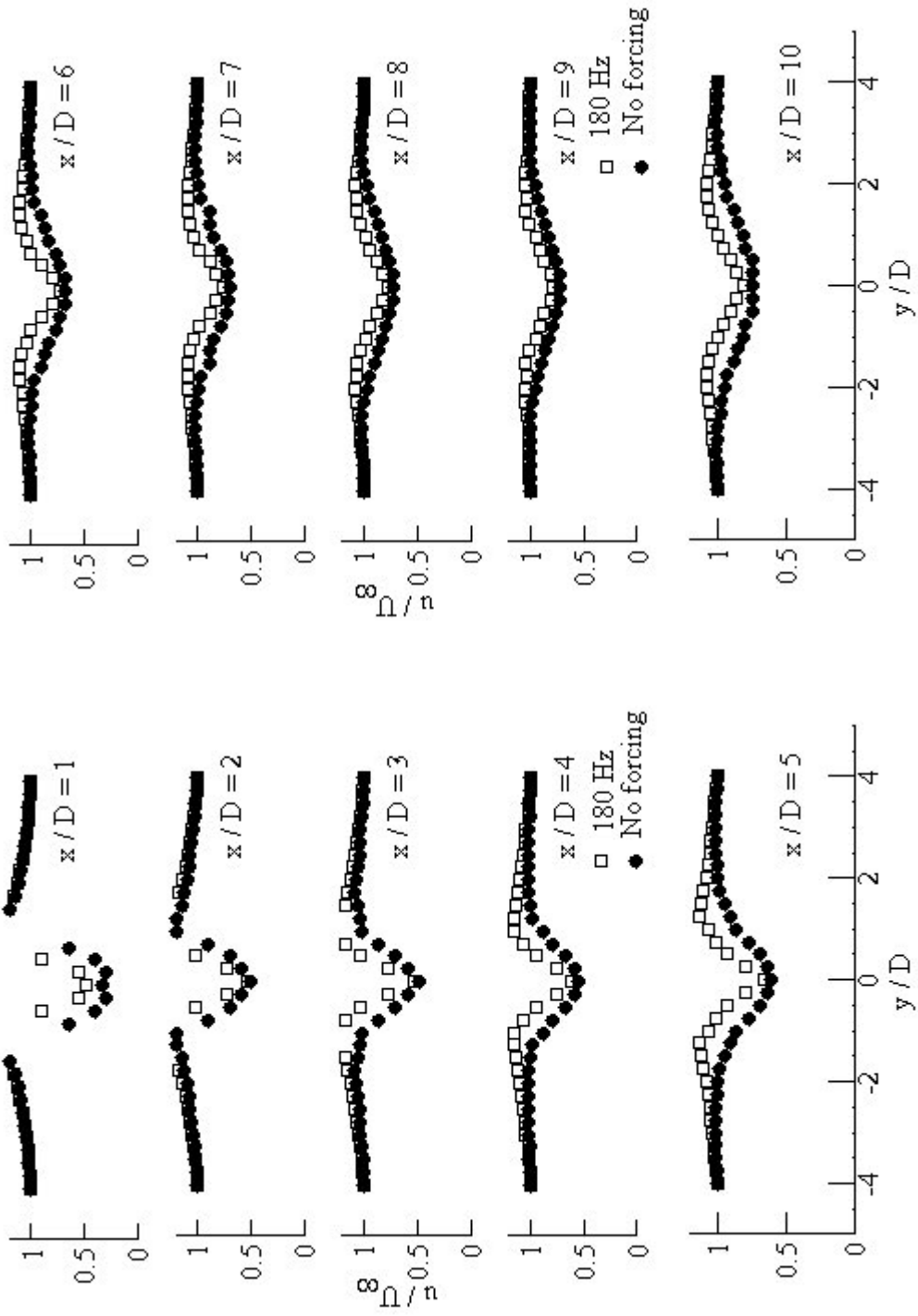


Figure 3.3: Cross sectional distribution of mean velocity, $Re=45,000$

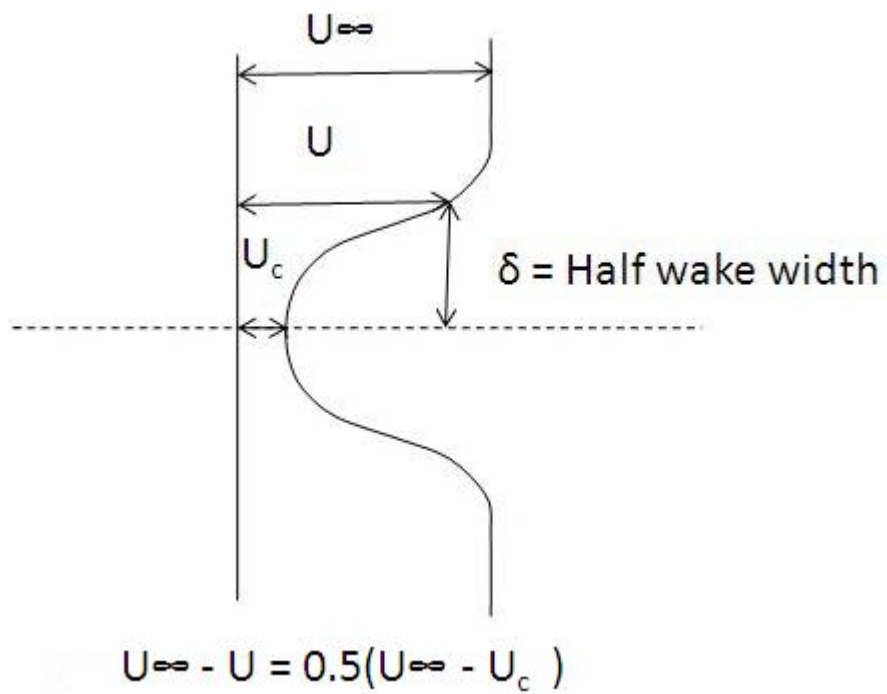
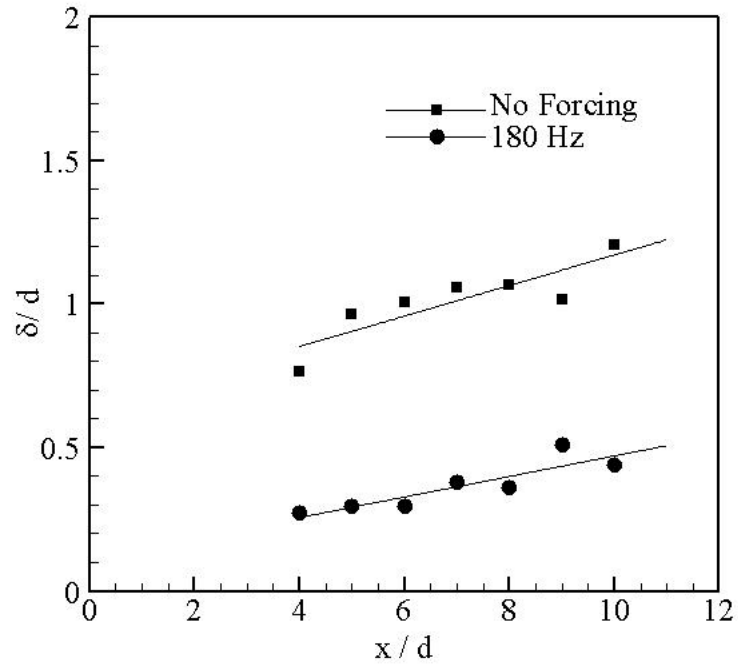
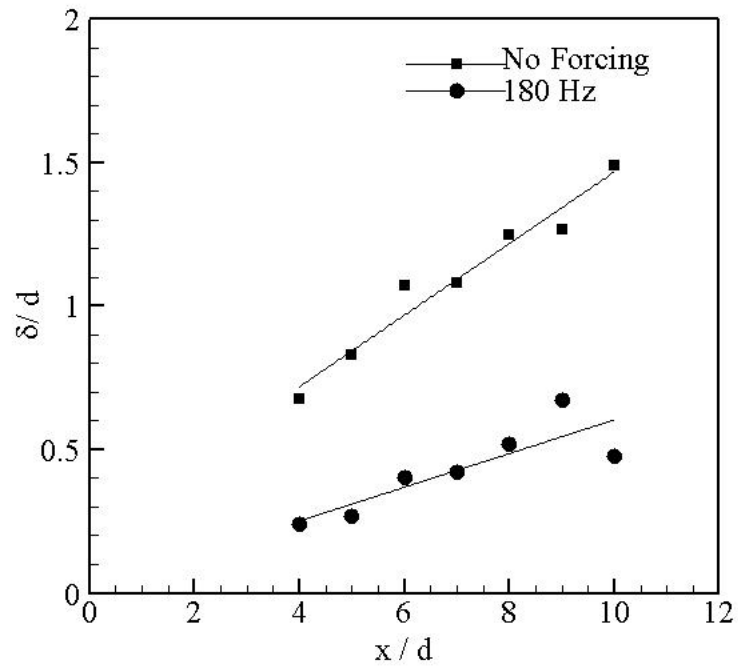


Figure 3.4: Half wake width



(a) $Re=24,000$



(b) $Re=45,000$

Figure 3.5: Variation of half wake width

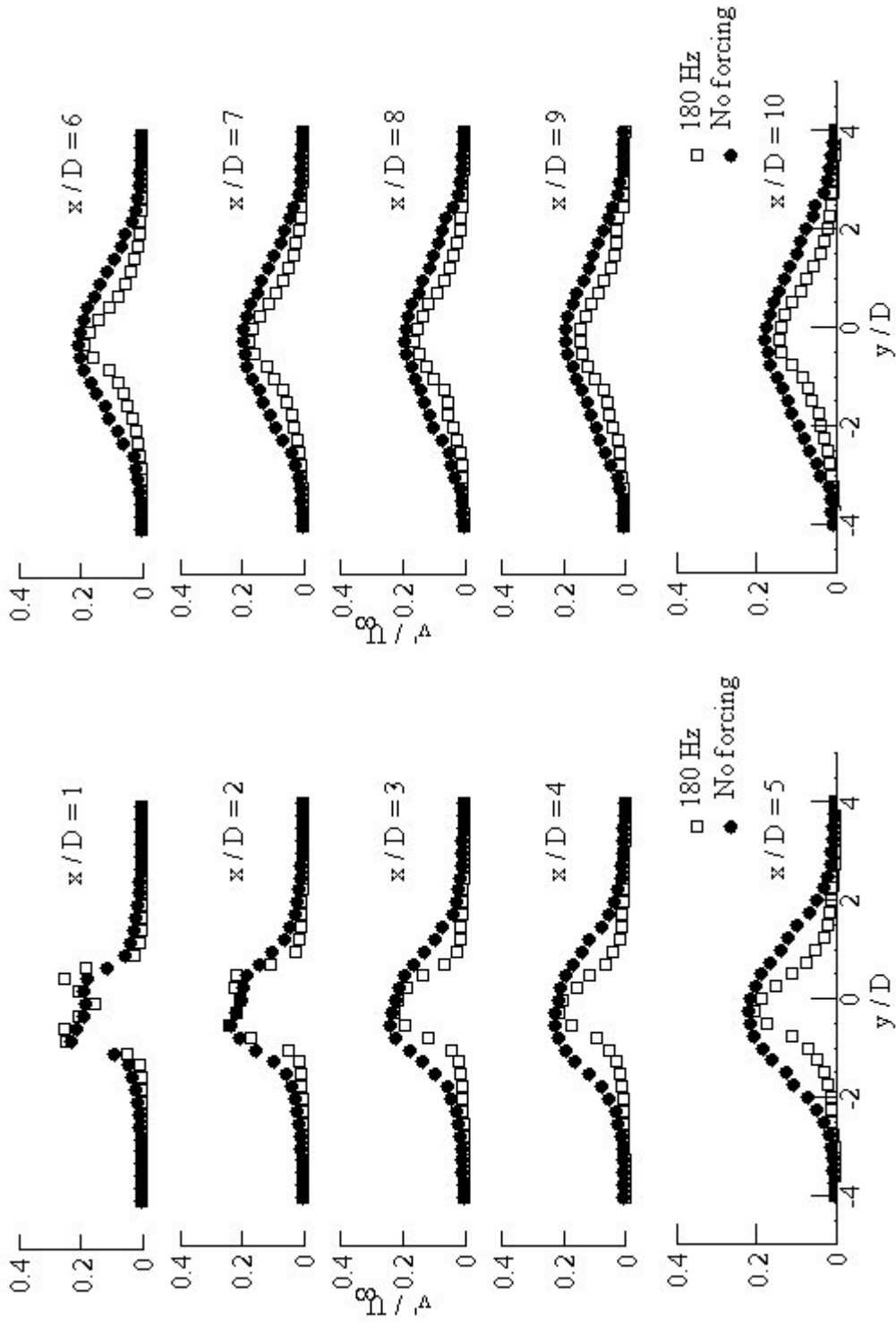


Figure 3.6: Cross sectional distribution of velocity fluctuation v' , $Re=24,000$

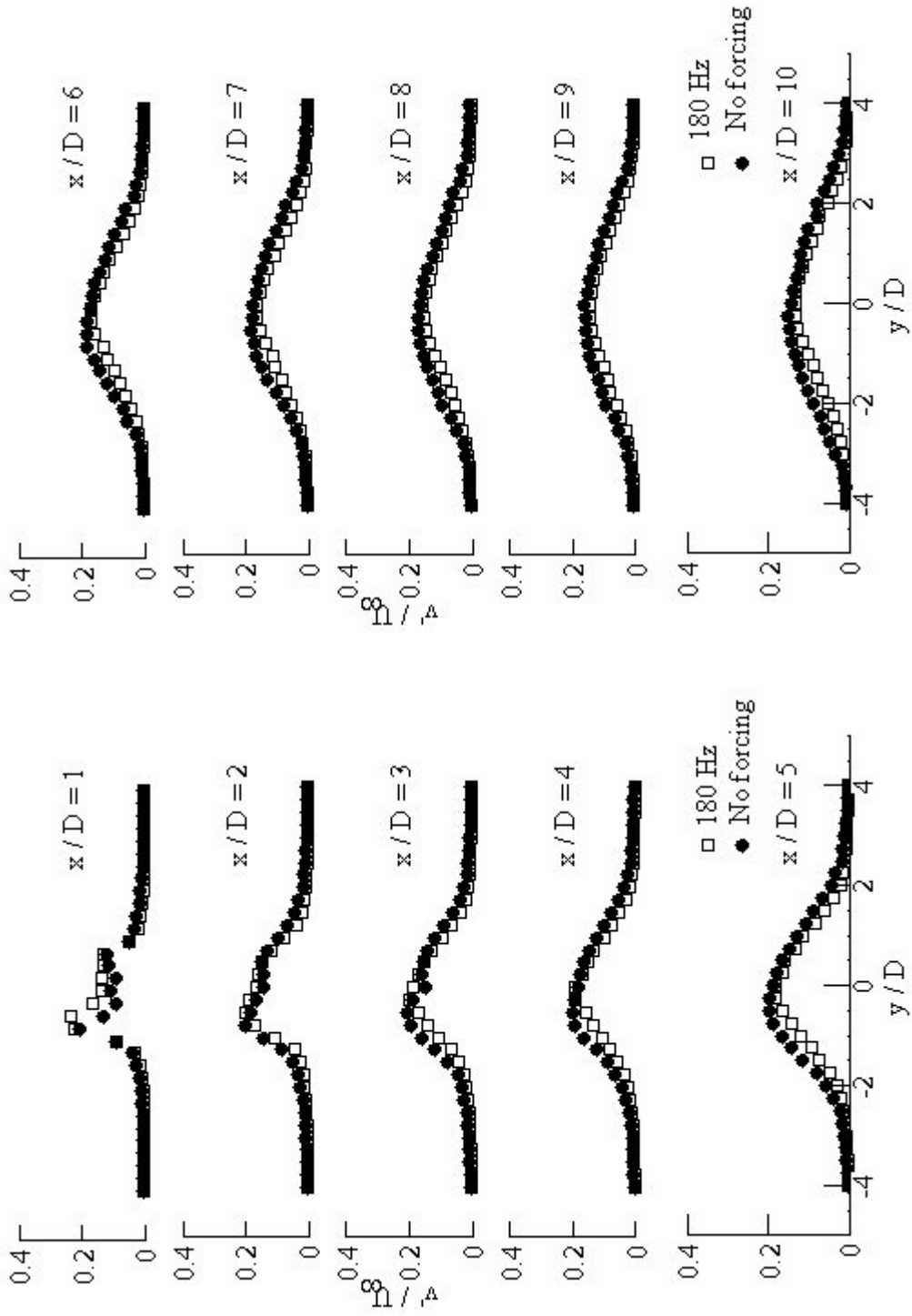


Figure 3.7: Cross sectional distribution of velocity fluctuation v' , $Re=45,000$

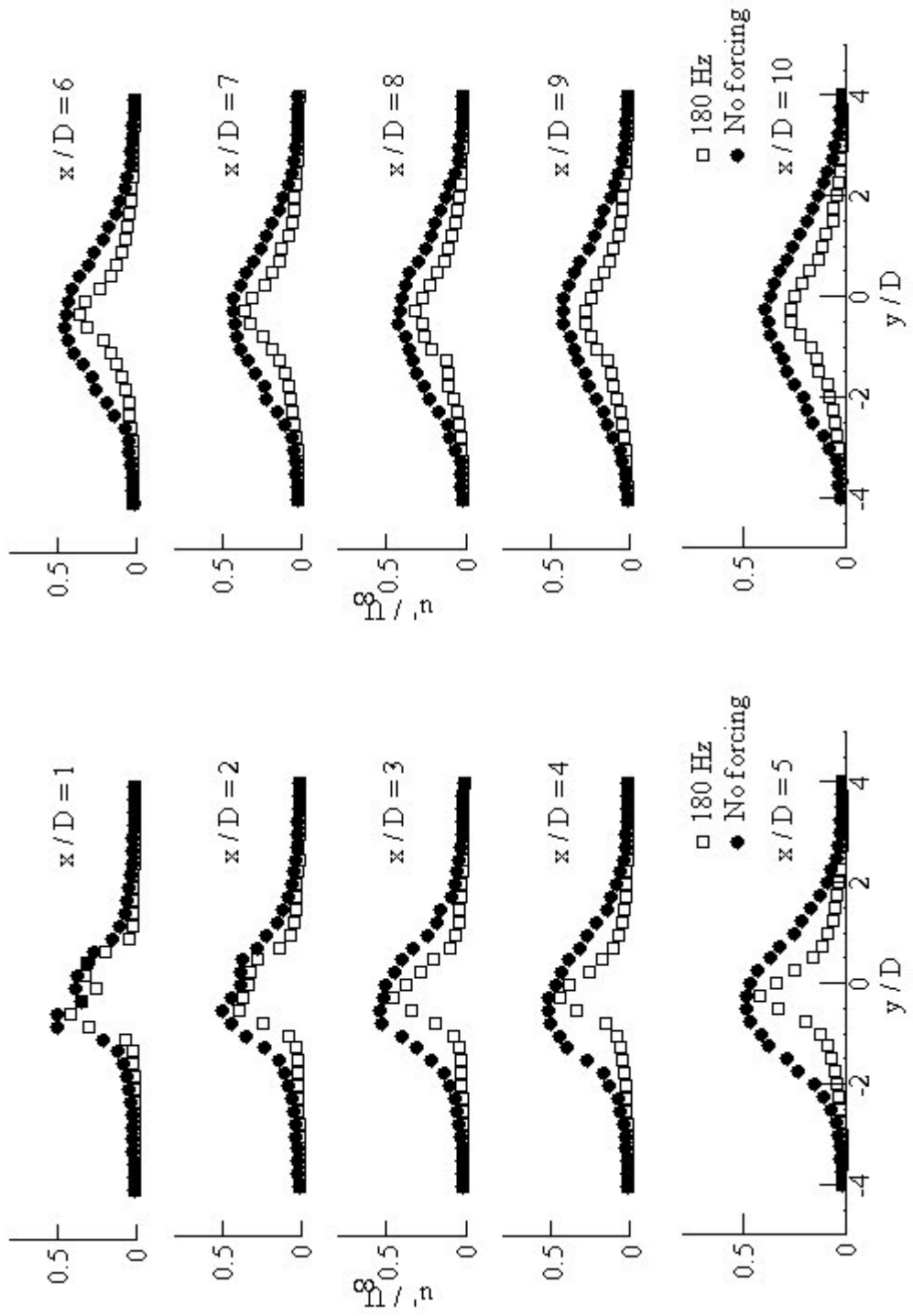


Figure 3.8: Cross sectional distribution of velocity fluctuation u' , $Re=24,000$

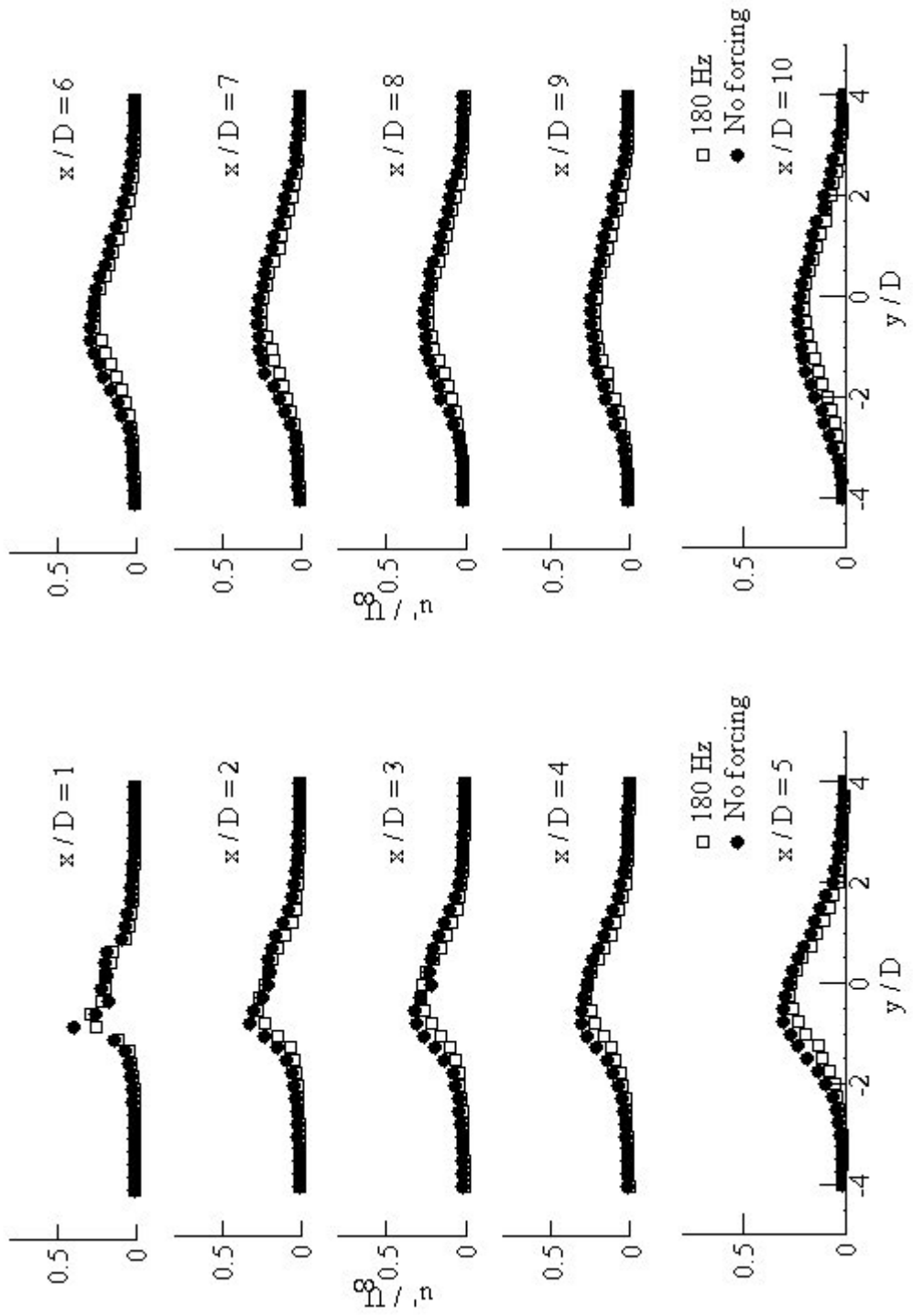


Figure 3.9: Cross sectional distribution of velocity fluctuation u' , $Re=45,000$

3.4 Characteristics of the flow field:

In order to understand the overall effect of the forcing on the wake of the circular cylinder the magnitude of the shedding peak was determined from the spectrum plot at each data points (33 x 10), taken by traversing the x wire in the whole wake. The data was used to plot the contours as shown in figure 3.10. The contour plot signifies the distribution of energy in the shedding component in the entire wake up to $\frac{x}{d} = 10$. This distribution is useful in determining how the vortical structures develop in the near wake of a circular cylinder under forcing compared to that of no forcing case. In the no forcing case, the maximum of the energy was contained in the two shear layers emanating from the top and bottom side of the cylinder. This was around $\frac{y}{d} = \pm 0.5$ and ranged up to $\frac{x}{d} = 2$ approximately. This was the region where spectrum of the hot wire signal registered strongest peaks of the vortex shedding frequency. In the center of the wake as two vortices from the top and bottom side of the cylinder met each other, the peak in the spectrum plot shifted to $2f_{s0}$, where f_{s0} is the vortex shedding frequency. Gradually these structures convected downstream and the energy content in the main shedding component reduced which signifies distribution of the energy to smaller scales. On the other hand, the introduction of the forcing with 180 Hz excitation, through the top and bottom slit of the circular cylinder had some remarkable effect on the wake. From figure 3.10 it is evident the energy of the main shedding component was not localized around the separating shear layer any more in case of 180 Hz forcing, rather it was distributed in the wake in a uniform manner. Also the wake had got narrower as indicated by the vertical width of the contour plot. This is attributed to the disturbance introduced in the flow through the sinusoidal slits which have broken down the regular development of the vortices from the two sides. Consequently the shear layer now consists of smaller diameter vortices instead of the large vortical structures. The velocity in the shear layer also increased as it consisted of smaller diameter eddies which had greater flow velocity. Figure 3.11 shows the energy distribution in the shedding peak for different cases in

the higher Reynolds number case. The corresponding contour levels can be estimated from the colorbar in the figure.

3.5 Kinetic energy in the wake:

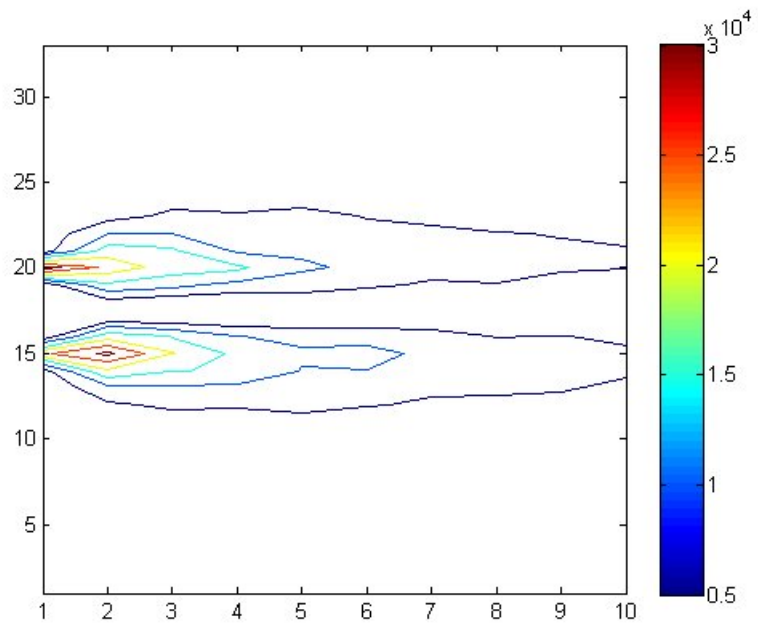
The smaller eddies carried less energy downstream than the bigger eddies. Along with this as the uniformity in the flow velocity increased, the wake narrowed down downstream. These two factors contributed towards the suppression of the normal and stream wise velocity fluctuations, which also implies that the available turbulent kinetic energy decreased downstream due to the forcing. This suppression due to forcing was more pronounced in the lower Reynolds number case as evident from the figure 3.12 which shows the distribution of turbulent kinetic energy in the wake ($TKE = \frac{1}{2} \frac{\overline{u'^2} + \overline{v'^2}}{U_\infty^2}$). In case of Re of 45,000, the kinetic energy of turbulence came down due to forcing with 180 Hz disturbance at $\frac{x}{d} = 6$ to 8. But no marked difference was observed thereafter (figure 3.13). For this calculation, the contribution of in the wake is only retained though Harsha and Lee [45] have suggested using $\overline{v'^2} = \overline{w'^2}$ for turbulent kinetic energy computation.

3.6 Wake preservation:

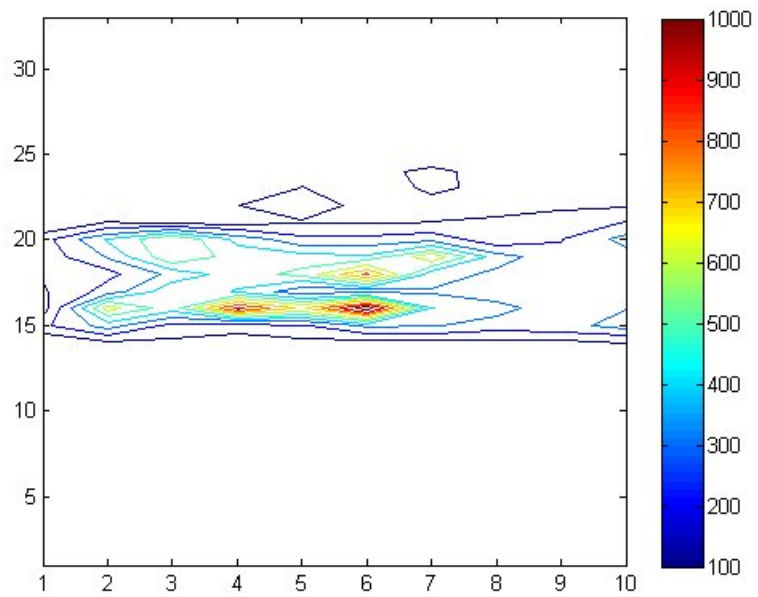
The wake behind a bluff body can be broadly categorised in two regions

1. Near wake region
2. Far wake region

Extensive studies have been carried out to characterise the far wake ([44],[43]). The wake can be said to have reached an asymptotic state when all flow properties reach an universal distribution which is independent of the initial condition. The mean flow development in the far wake which is generally at a large downstream distance from the bluff body, is characterised by the drag of the body. On the other hand the near wake (just behind the bluff body) is strongly influenced by the characteristics of the body as well as the upstream flow condition. A change in turbulence structure of the flow takes place in the near wake.

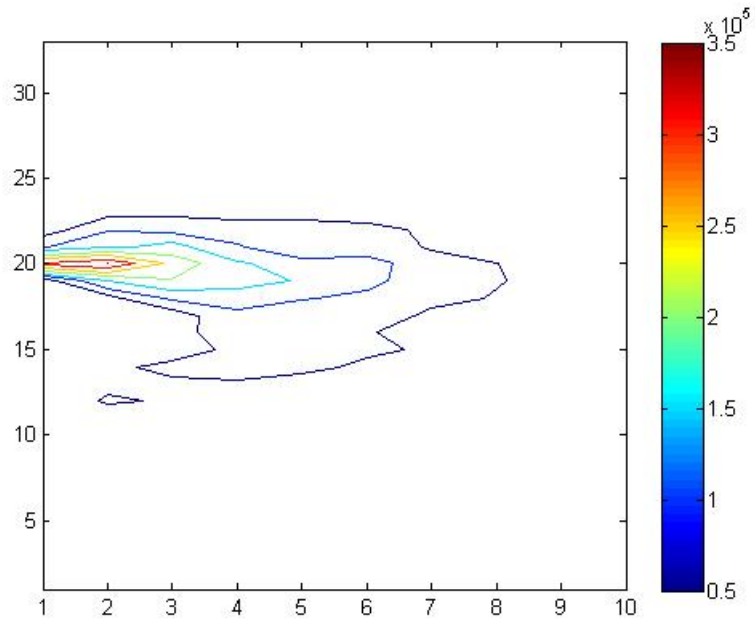


(a) No forcing

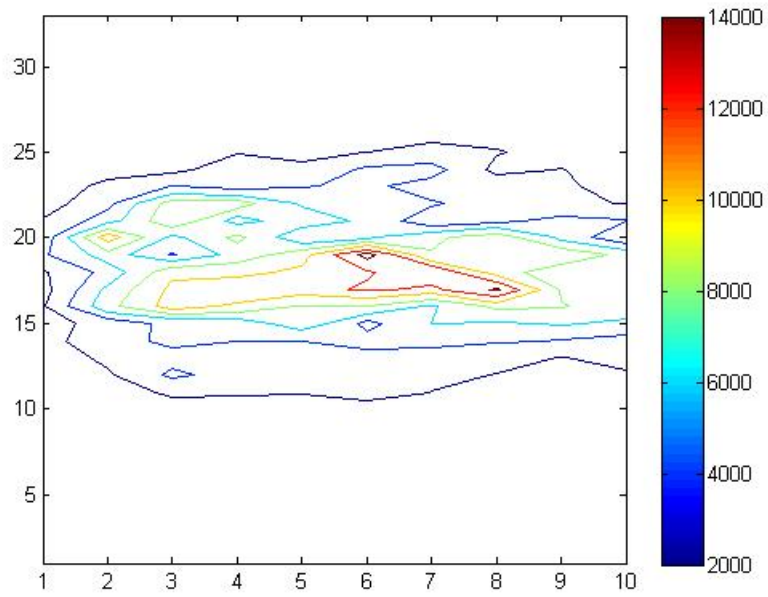


(b) 180 Hz

Figure 3.10: Contour plot of the magnitude of the shedding peak, $Re=24,000$



(a) No forcing



(b) 180 Hz

Figure 3.11: Contour plot of the magnitude of the shedding peak, $Re=45,000$

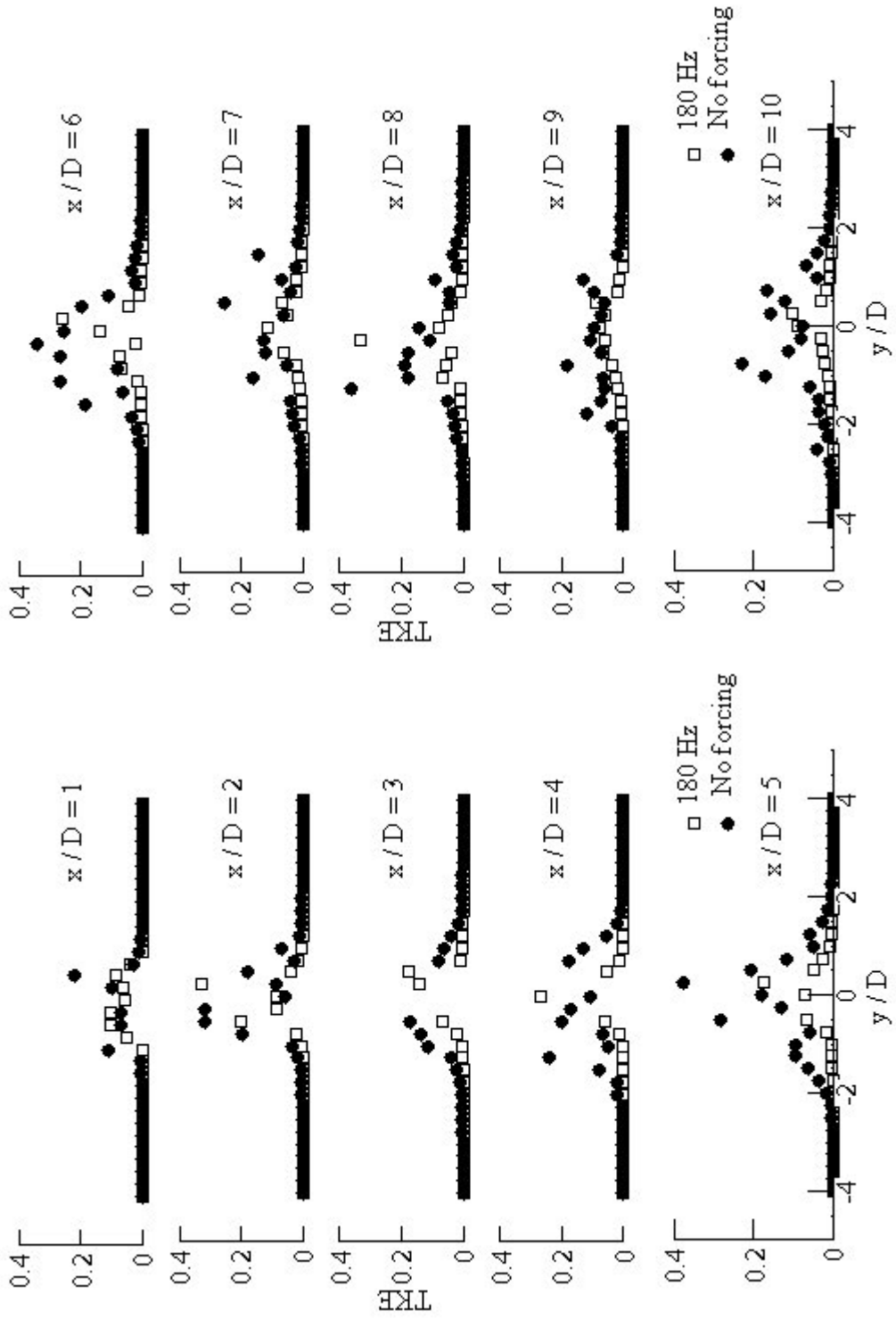


Figure 3.12: Cross sectional distribution of turbulent kinetic energy, $Re=24,000$

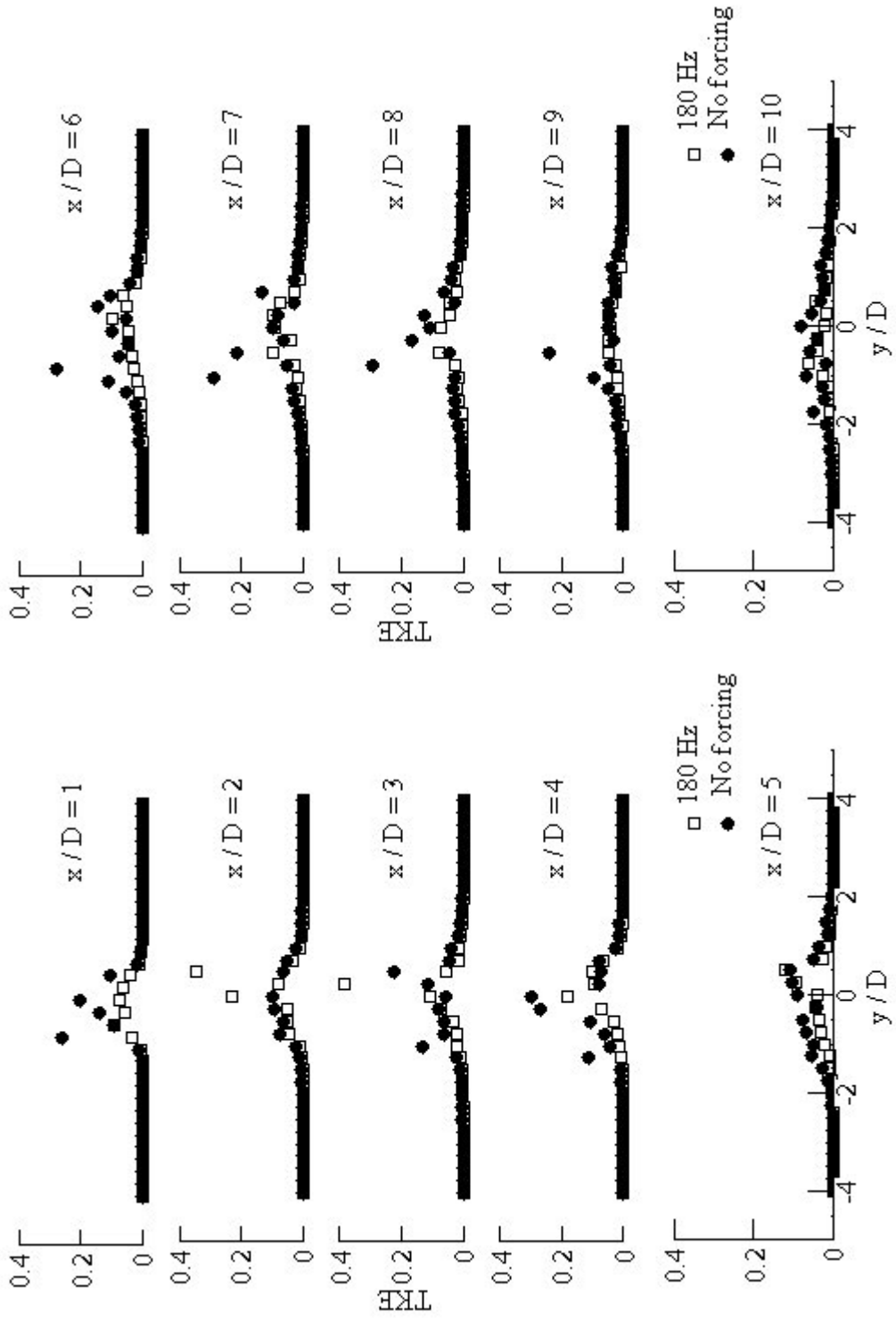


Figure 3.13: Cross sectional distribution of turbulent kinetic energy, $Re=45,000$

The wall of the bluff body generates vorticity and that gets advected with the mean flow. In the near wake a free turbulence condition exists. The near wake is also signified by the adjustments of pressure fields and by viscid inviscid interaction. The wake is supposed to have reached a self preserving state when these following asymptotic trends are reached.

$$W_0 \propto X^{-\frac{1}{2}}$$

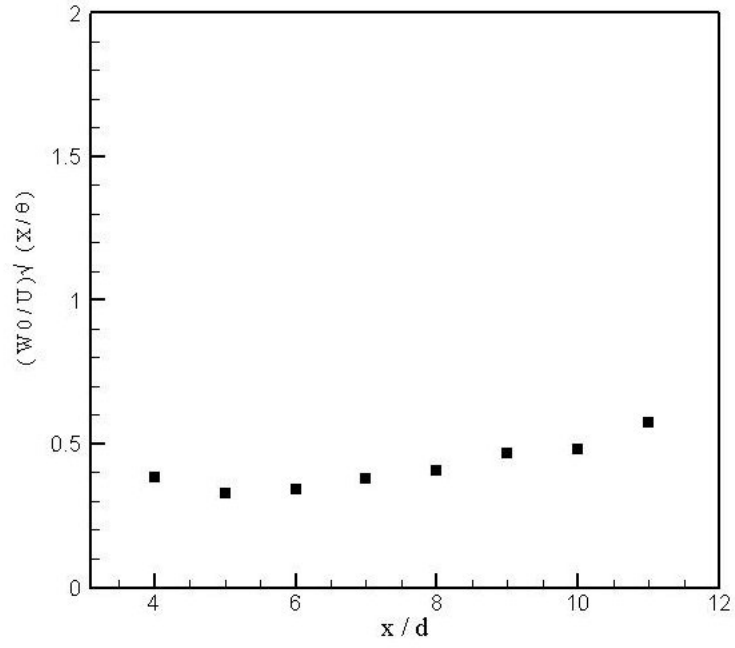
$$b \propto X^{\frac{1}{2}}$$

W_0 is the maximum velocity defect and b is the half wake width. Also a self preserving wake is characterised by the parameter $(\frac{W_0}{U})\sqrt{\frac{X}{\theta}}$. Far away from the wake this equilibrium parameter attains an universal value of 1.63. The term θ is called the wake momentum thickness which is defined as $\theta = \int_{-\infty}^{\infty} \frac{U}{U_{\infty}}(1 - \frac{U}{U_{\infty}})dy$. Thus the behavior of the measured values of the similarity parameters indicate the manner the wake is reaching the asymptotic state. The distribution of this parameter in the stream wise direction for different forcing conditions are shown in figure 3.14 to 3.19.

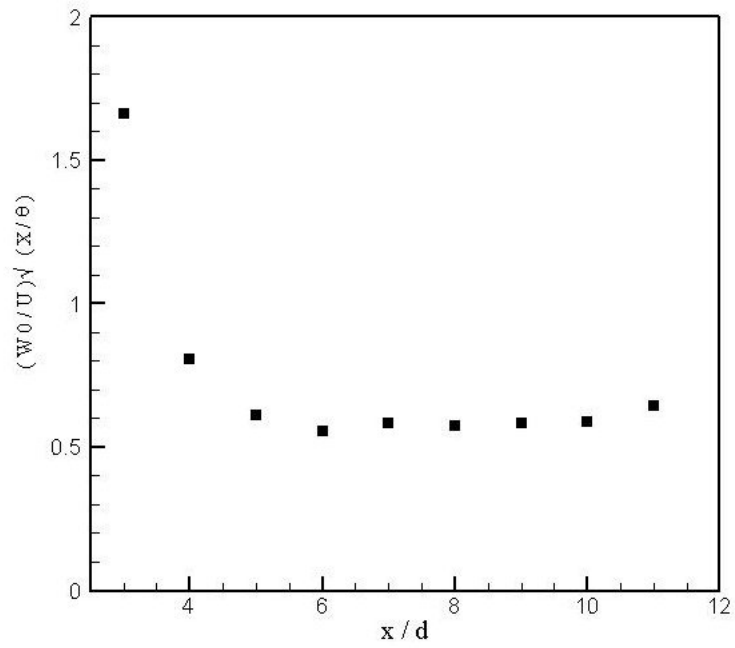
For Reynolds number of 24,000 case, the distribution of the values of $(\frac{W_0}{U})\sqrt{\frac{X}{\theta}}$ in the noforcing case indicates, in the near wake, upto $\frac{x}{d} = 11$ the asymptotic value has not been reached. But the trend of the values towards the asymptotic limit is evident. When the three dimensional disturbance of 180 Hz was forced, this trend was hampered. The local maxima of the similarity parameter around $\frac{x}{d} = 5$ can be attributed to the increase in velocity defect (w) for the forcing case. As was pointed out in section 3.2 the centerline velocity was found to decrease in case of forcing with 180 Hz disturbance. The same explanation can be applied to the higher Reynolds number also (Figure 3.17 and 3.19).

3.7 Wake formation length:

The wake formation length indicates the point in the wake where the velocity fluctuation reaches a maximum value. It can also be defined as the point of maximum fluctuation of the second harmonic component. It can be noted that in the centerline of the wake, the second harmonic component of the shedding has the maximum energy but with a frequency double the shedding frequency. It is because in the centerline of the wake vortices from

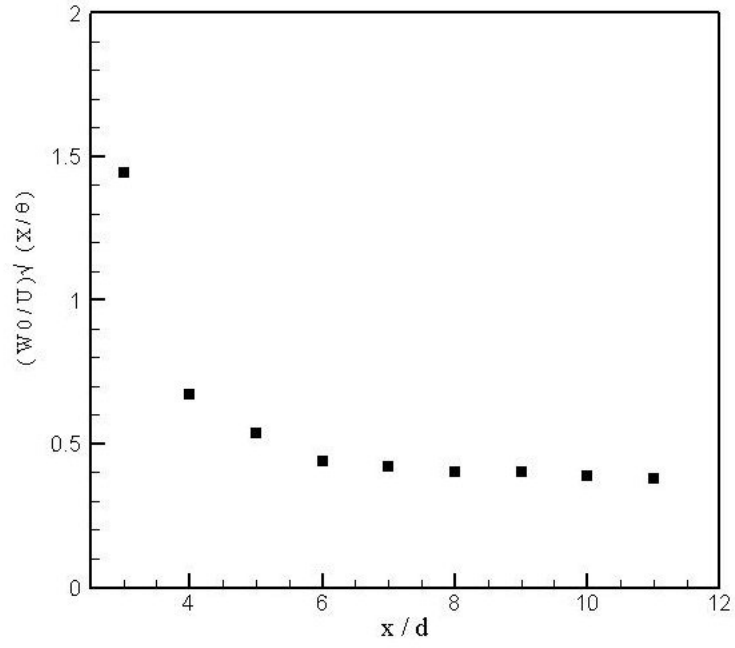


(a) Noforcing

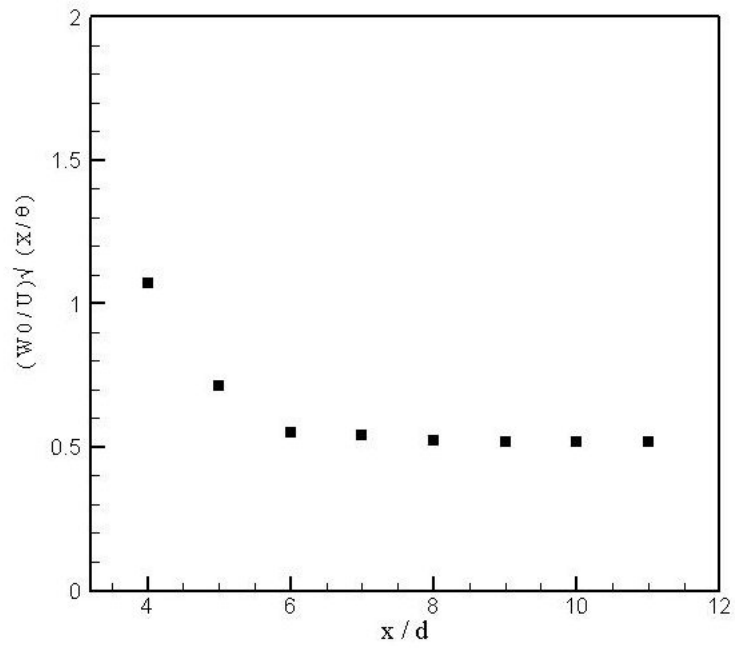


(b) 25 Hz

Figure 3.14: Similarity parameter in wake, $Re=24,000$

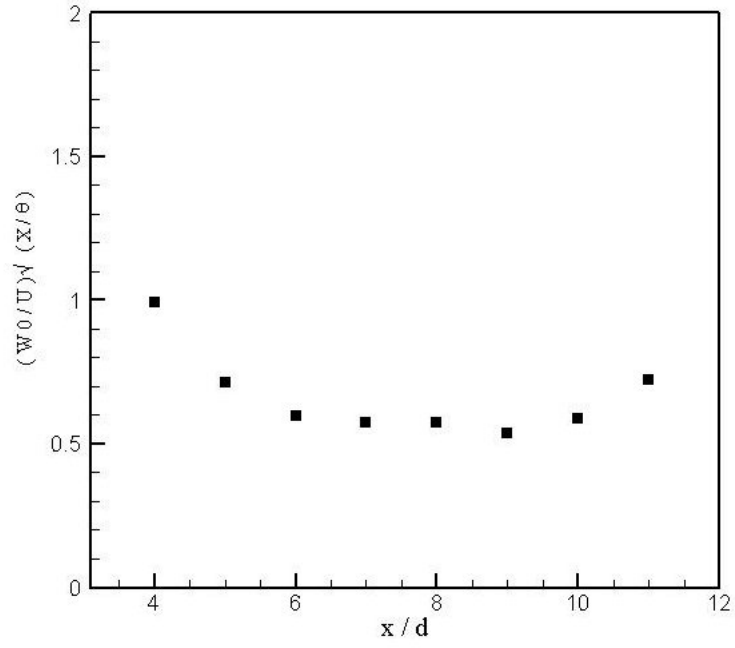


(a) 45 Hz

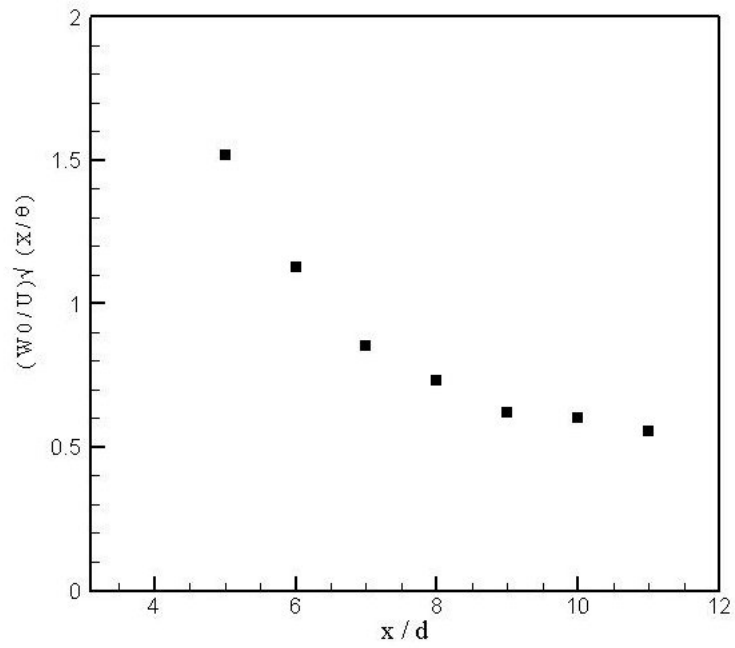


(b) 50 Hz

Figure 3.15: Similarity parameter in wake, $Re=24,000$

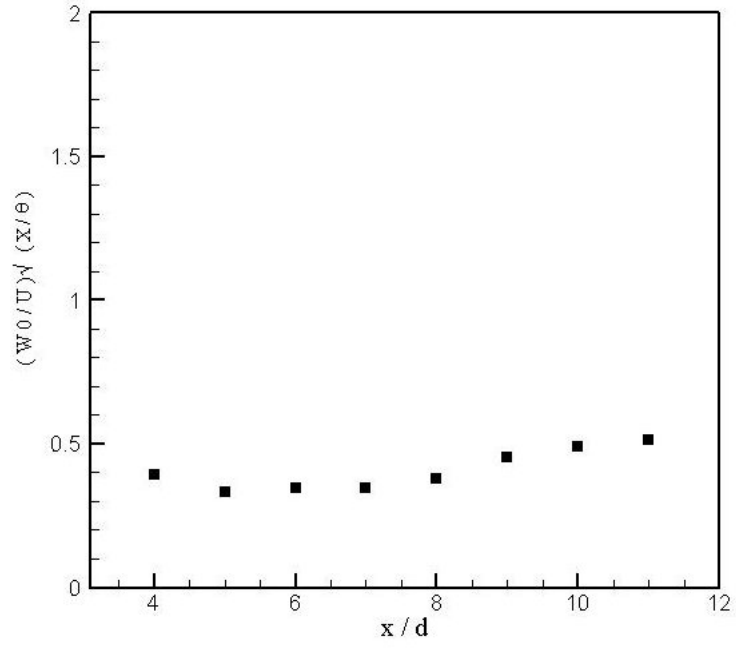


(a) 60Hz

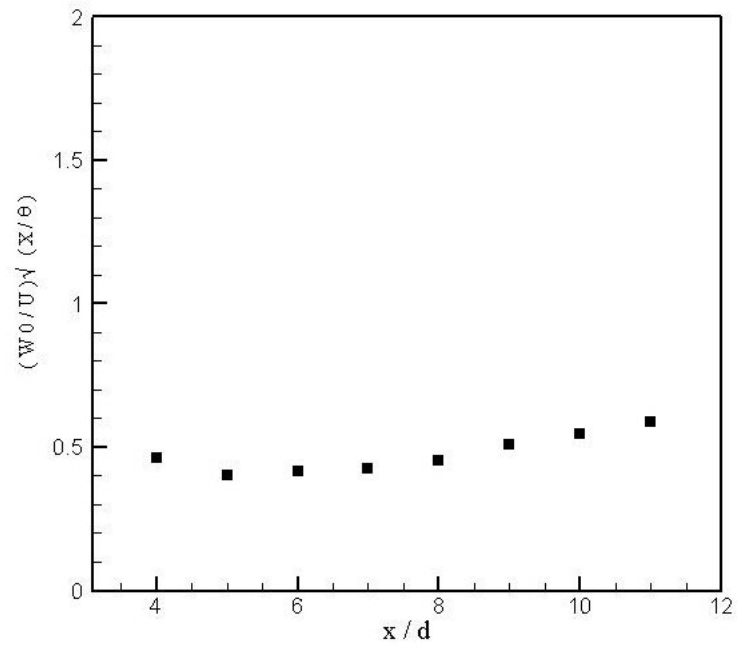


(b) 180 Hz

Figure 3.16: Similarity parameter in wake, $Re=24,000$

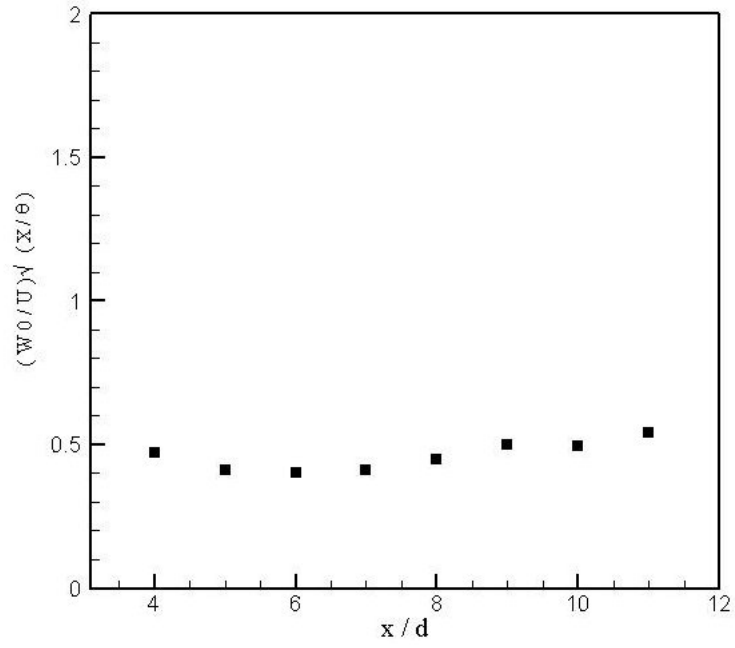


(a) Noforcing

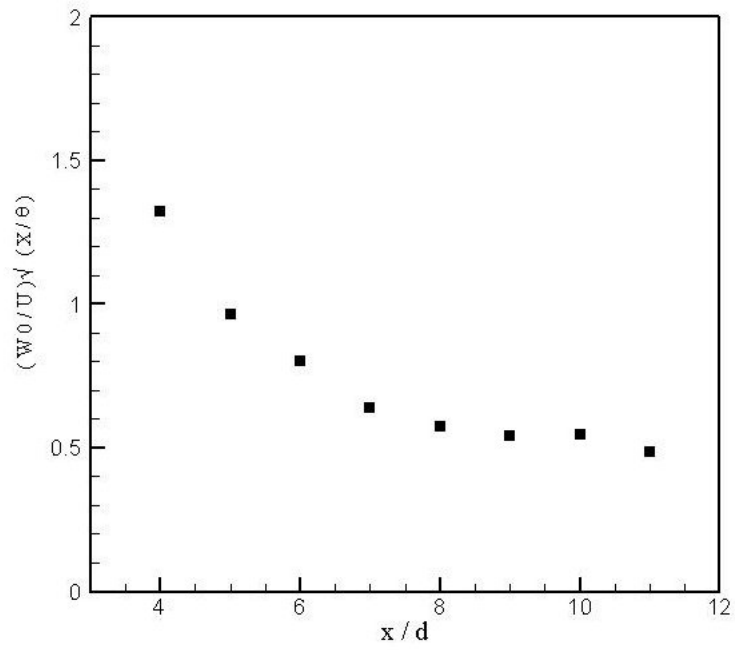


(b) 38 Hz

Figure 3.17: Similarity parameter in wake, $Re=45,000$

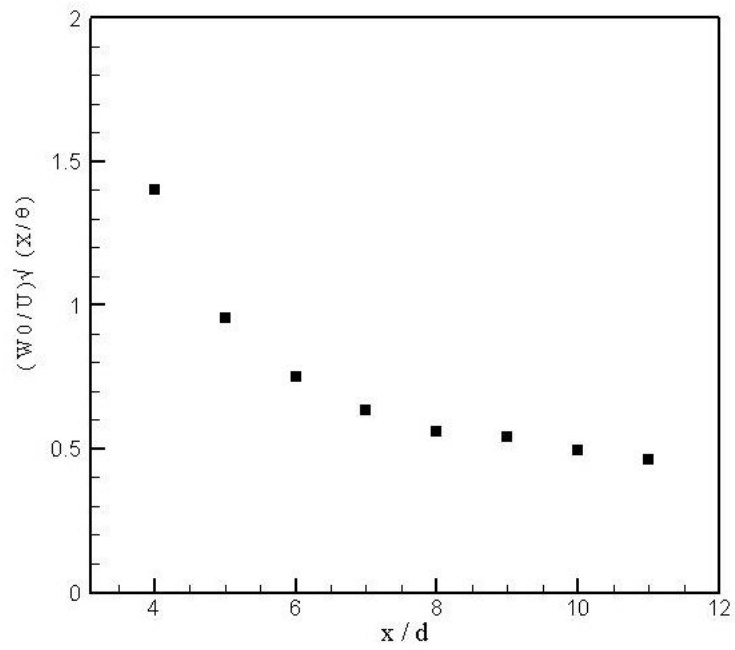


(a) 76 Hz



(b) 156 Hz

Figure 3.18: Similarity parameter in wake, $Re=45,000$

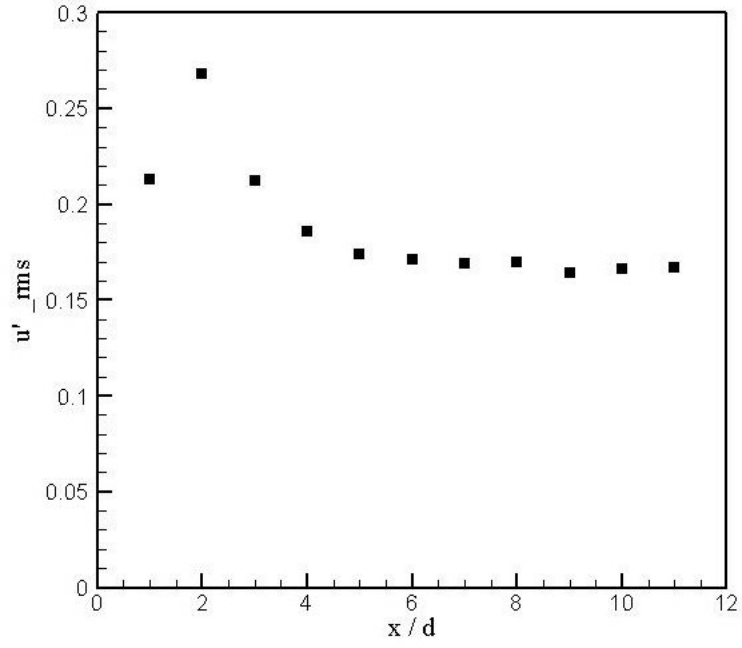


(a) 180Hz

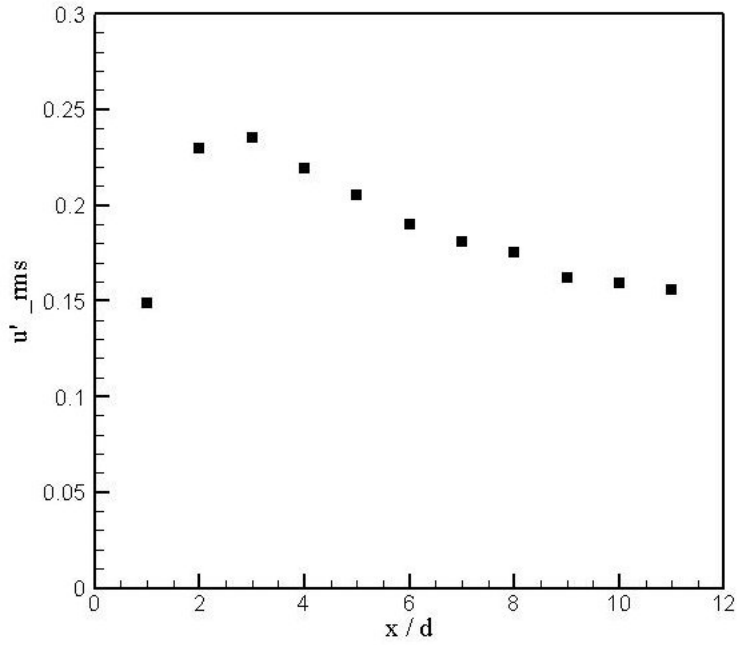
Figure 3.19: Similarity parameter in wake, $Re=45,000$

both side interact with each other. Another definition of wake formation length says it is the point where the outside fluid crosses the wake centerline for the first time. Here the streamwise velocity fluctuation in the centerline of the wake has been considered for finding the wake formation length.

Figure 3.20 to 3.25 shows the wake formation lengths for different cases of forcing. For the noforcing case(Figure 3.20) in Reynolds number 24,000 case, the wake formation length was found to be around $2d$.As the forcing frequency increased the wake formation length was found to increase gradually.But the corresponding maximum fluctuation level came down.This is in accordance with section 3.3 where it was shown that the application of forcing reduces the fluctuation level of velcocity components in the wake. Figure 3.22 shows that when 180 Hz forcing was applied the peak in the fluctuation of streamwise velocity attained its minimum value and the corresponding point of maximum fluctuation in the centerline of the wake shifted to around $4d$. This increase in wake formation length is attributed to the local disturbance created by the forcing which disrupts the formation of a regular vortex street. As the development of large scale karman vortices was disturbed, the character of the regular wake was changed. This is evident in the change in the wake formation length. The same reason holds true for the higher Reynolds number case also. In this case the wake formation length was shifted to around $3d$ for forcing with 180 Hz (Figure 3.25)

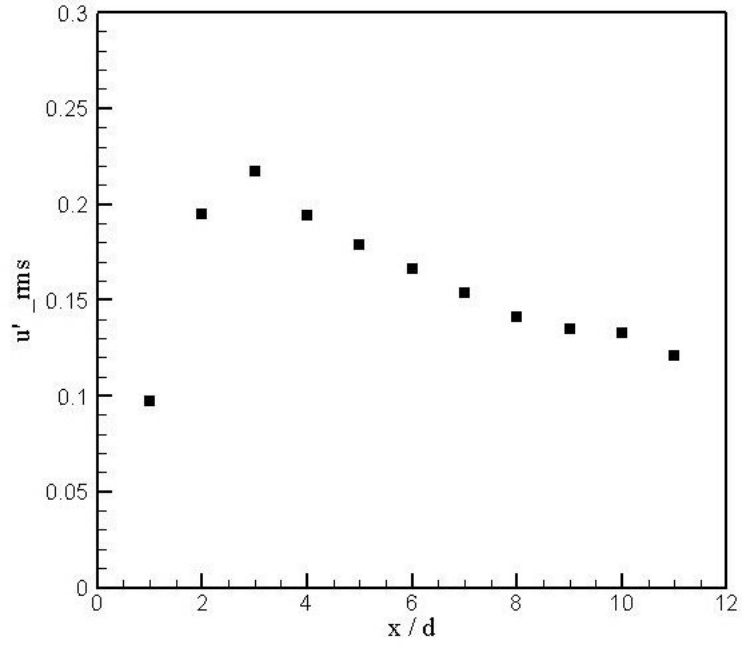


(a) No forcing

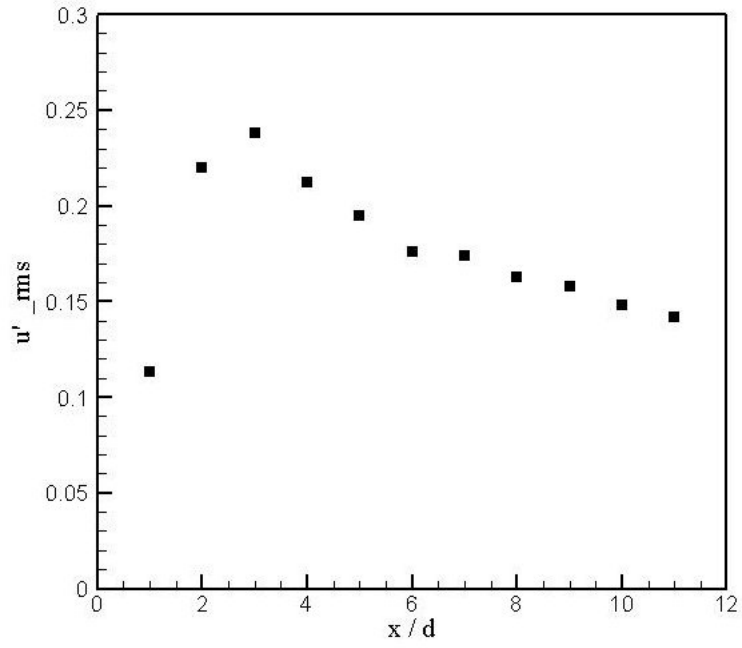


(b) 25 Hz

Figure 3.20: Wake formation length, $Re=24,000$

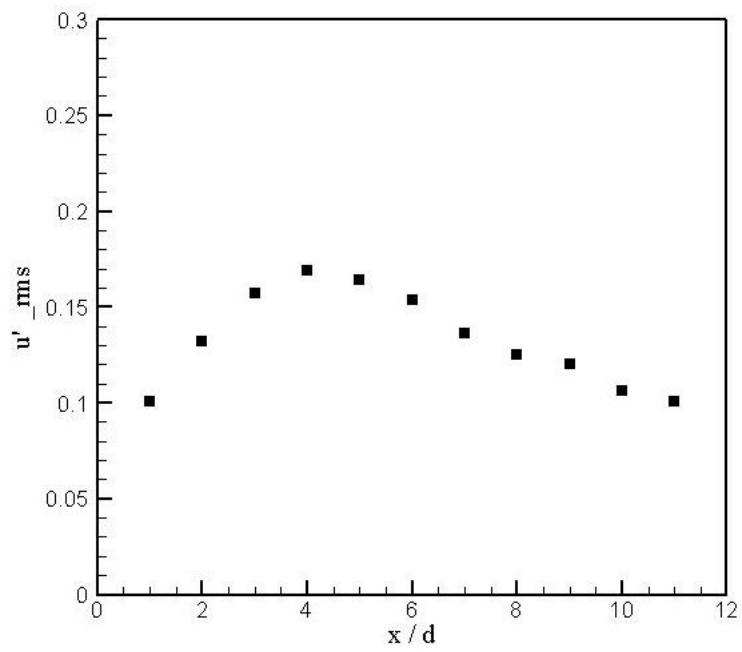


(a) 50 Hz



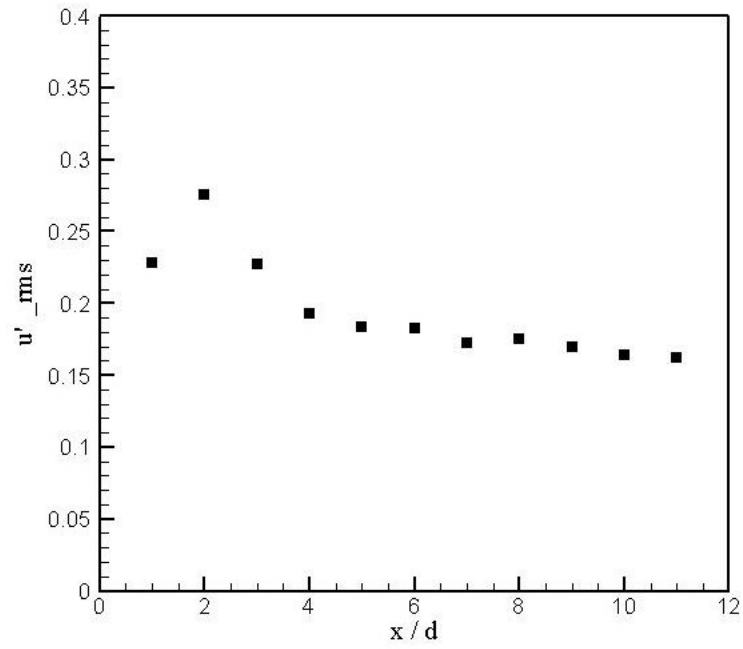
(b) 60 Hz

Figure 3.21: Wake formation length, $Re=24,000$

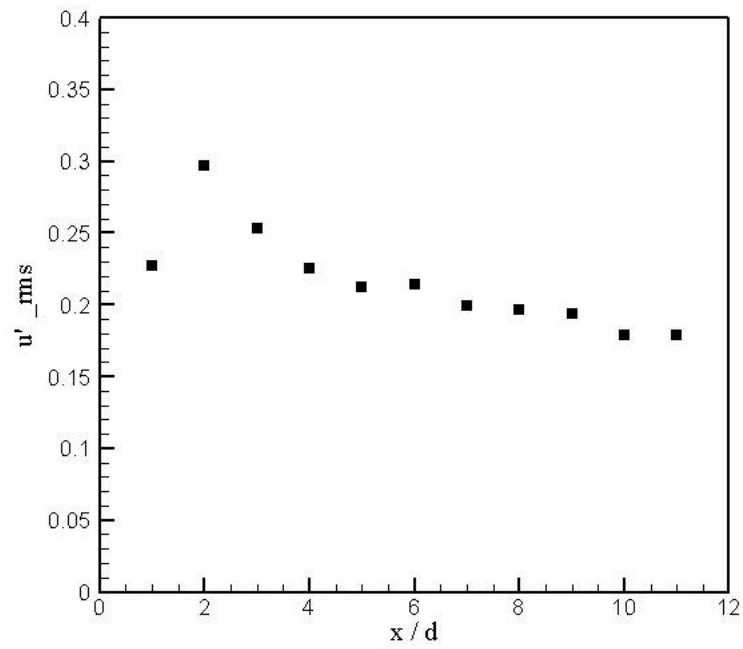


(a) 180 Hz

Figure 3.22: Wake formation length, $Re=24,000$

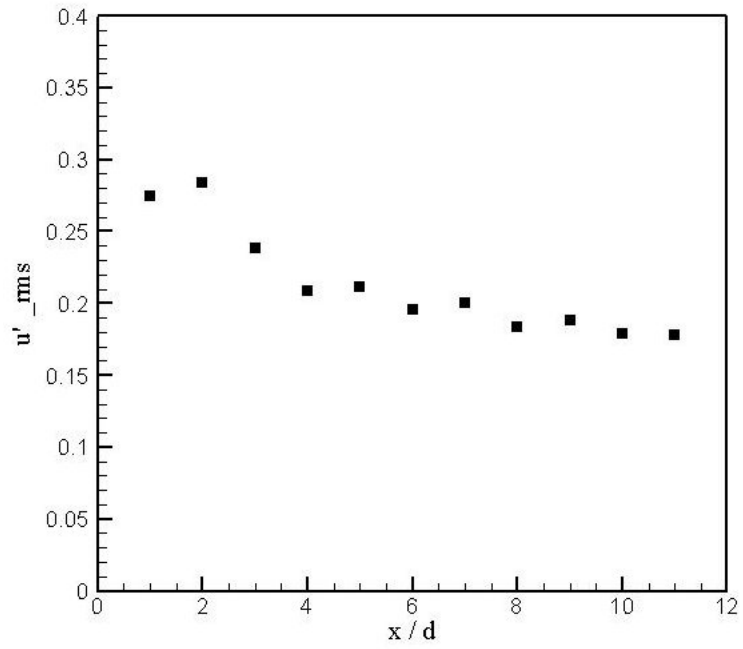


(a) No forcing

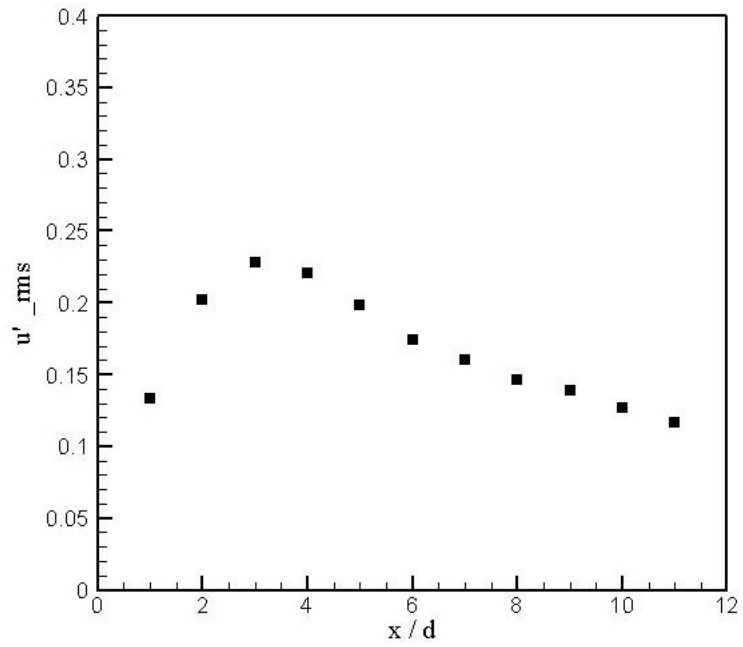


(b) 38 Hz

Figure 3.23: Wake formation length, $Re=45,000$

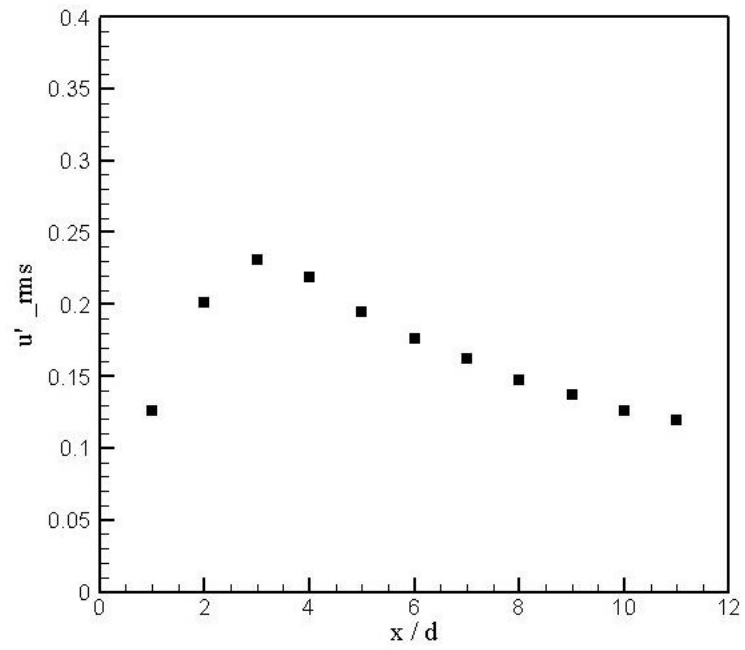


(a) 76 Hz



(b) 156 Hz

Figure 3.24: Wake formation length, $Re=45,000$



(a) 180 Hz

Figure 3.25: Wake formation length, $Re=45,000$

CHAPTER 4

CONCLUSION

The wake of a circular cylinder was investigated with a three dimensional disturbance, caused by forcing from two loud speakers, which was introduced in the flow field through two sinusoidal slits located on two diametrically opposite direction on the cylinder surface. Experiment was done at two different Reynolds numbers. For Reynolds number 24,000 (shedding frequency about 50 Hz) it was observed that a forcing frequency of 60 Hz was able to eliminate the shedding peak completely. For Reynolds number 45,000 (shedding frequency about 78 Hz) the shedding component was eliminated by 100 Hz forcing. But in this case a forcing with 76 Hz excitation resulted in strengthening of the peak. The mean velocity plot showed that the wake width gets considerably narrowed in case of a forcing with 180 Hz excitation which also reduced the drag for the low Reynolds number case. Previous research, which introduced two dimensional disturbances through a straight slit, have shown that in lower Reynolds numbers (typically 9,000) a forcing frequency which is almost four times the shedding frequency has to be selected for complete elimination of the von Karmann shedding component. Results obtained from this experiment lead to the conclusion that even a forcing frequency less than four times shedding frequency can eliminate the shedding peak in a turbulent wake of a circular cylinder. Provided the blowing coefficient is sufficient to create three dimensional disturbance which in effect breaks the vortex street into smaller eddies. Due to this, the energy in the wake was uniformly distributed in the smaller structures from the main shedding component. The acceleration of the two separating shear layers due to the forcing narrowed the wake thus registering the uniformity in velocity.

BIBLIOGRAPHY

- [1] Berger,E.,Wille,R.,1972.Periodic Flow Phenomena.Annual Review of Fluid Mechanics.11:313-340
- [2] Bearman,PW.,1984.Vortex Shedding From Oscillating Bluff Bodies.Annual Review of Fluid Mechanics.16:195-222
- [3] Oertel,H.,1990.Wakes Behind Blunt Bodies.Annual Review of Fluid Mechanics.22:539-564
- [4] Williamson, CHK.,1996.Vortex Dynamics in the Cylinder Wake.Annual Review of Fluid Mechanics.28:477-539
- [5] Hayakawa,M.,Hussain,F.,1989.Three Dimensionality in a Plane Turbulent Wake.Journal of Fluid Mechanics.206:375-404
- [6] Bloor,M.S.,1964.The Transition to Turbulence in the Wake of a Circular Cylinder.Journal of Fluid Mechanics.19:290-303
- [7] Wei,T.,Smith,C.R.,1986.Secondary Vortices in the Wake of Circular Cylinder.Journal of Fluid Mechanics.169:513-533
- [8] King,R.,1977.A Review of Vortex Shedding Research and its Application.Ocean Engineering.4:141-172
- [9] Bishop, R. E. D., Hassan, A. Y., 1964. The Lift and Drag Forces on a Circular Cylinder in a Flowing Fluid. Proceedings Royal Society (London), Series A 277, 32-50
- [10] Blevins, R. D., 1990. Flow Induced Vibration, 2nd edition, Van Nostrand Reinhold, NY
- [11] Fung, Y. C., 1960. Fluctuating Lift and Drag Acting on a Cylinder in a Flow at Supercritical Reynolds Numbers. Journal of Aerospace Sciences 24, 801-804
- [12] Gerrard, J. H., 1961. An Experimental Investigation of Oscillating Lift and Drag of a Circular Cylinder Shedding Turbulent Vortices. Journal of Fluid Mechanics 11, 244-256.
- [13] Jordan, S. K., Fromm, J. E., 1972. Oscillatory Drag, Lift and Torque on a Cylinder in a Uniform Flow. Physics of Fluids 15, 371-376
- [14] Schmidt, L. V., 1965. Measurements of Fluctuating Loads on a Circular Cylinder. Journal of Aircraft 2, 49-55.

- [15] Bays-Muchmore, B., Ahmed, A., 1993. On Streamwise Vortices in the Turbulent Wakes of Cylinders. *Physics of Fluids* 5,387-392
- [16] Choi,H., Jeon ,WP., Kim, J., 2008.Control of Flow over Bluff Body. *Annual Review of Fluid Mechanics* 40, 113-139
- [17] Ahmed, A.,Khan,M.J.,Bays-Muchmore,B., 1993. Experimental Investigation of Three Dimensional Bluff Body Wake.*AIAA Journal* 31, 559-563
- [18] Tanner, M., 1972.A Method for Reducing the Base Drag of Wings with Blunt Trailing Edge. *Aeronautical. Quarterly.*, 23(1), pp. 1523.
- [19] Bearman,PW.,Owen,JC.,1998.Reduction of Bluff Body Drag and Suppression of Vortex Shedding by the Introduction of Wavy Separation Lines.*Journal of Fluids and Structures.*12:123-130
- [20] Rodriguez,O.,1991.Base Drag Reduction by Control of the Three Dimensional Unsteady Vortical Structures.*Experiment in Fluids.*11:218-226
- [21] Tombazis, N., Bearman, P.W., 1997.A Study of Three Dimensional Aspects of Vortex Shedding from a Bluff Body with a Mild Geometric Disturbance. *Journal of Fluid Mechanics*, 330:85-112
- [22] Park, H.,Lee,D.,Jeon,WP.,Hahn,S.,Kim,J.,Kim,J.,Choi,J.,Choi,H.,2006.Drag Reduction in Flow Over a Two Dimensional Bluff Body with a Blunt Trailing Edge Using a New Passive Device. *Journal of Fluid Mechanics*, 563:389-414
- [23] Lee, S.,Kim,H.,1997.The Effect of Surface Protrusions on the Near Wake of a Circular Cylinder.*Journal of Wind Engineering and Industrial Aerodynamics*,69-71:351-361
- [24] Lim H, Lee S. 2002. Flow Control of Circular Cylinders with Longitudinal Grooved Surfaces. *AIAA Journal.* 10:202736
- [25] Lee,s.,Lim,H.,Han,M.,Lee,S.,2005.Flow Control of Circular Cylinder With a V Grooved Micro Riblet Film,*Fluid Dynamics Research*,37:246-266
- [26] Zhdanov,V.L.,Papenfuss,H.D.,2003.Bluff Body Drag Control By Boundary Layer Disturbance,*Experiments in Fluids*,34:460-466
- [27] Roshko A. 1955. On the Wake and Drag of Bluff Bodies. *Journal of Aeronautical Science.* 22:12432
- [28] Fujisawa,N.,Ikemoto,K.,Nagaya,K.,1998.Vortex Shedding Resonance From a Rotationally Oscillating Cylinder,*Journal of Fluids and Structures*,12:1041-1053
- [29] Cetiner O, Rockwell D. 2001. Streamwise Oscillations of a Cylinder in a Steady Current. Part 1: locked-on States of Vortex Formation and Loading. *J. Fluid Mech.* 427:128
- [30] Tokumaru PT, Dimotakis PE. 1991. Rotary Oscillatory Control of a Cylinder Wake. *J. Fluid Mech*,224:77-90

- [31] Kieft, R. N., Rindt, C. C. M., van Steenhoven, A. A., van Heijst, G. J. F., On the wake structure behind a heated horizontal cylinder in cross-flow, *Journal of Fluid Mechanics*, 486:189-211
- [32] Amitay M, Smith BL, Glezer A. 1998. Aerodynamic Flow Control Using Synthetic Jet Technology. 36th AIAA Aerosp. Sci. Meet., Reno, Nev., AIAA Pap. No. 980208
- [33] Roth J R, Sherman D M and Wilkinson S P 2000 Electrohydrodynamic Flow Control with a Glow Discharge Surface Plasma *AIAA J.*38:11729
- [34] Naim, A., Greenblatt, D., Seifert, A., Wignanski, I., 2007. Active Control of a Circular Cylinder Flow at Transitional Reynolds Numbers, *Journal of Flow Turbulence and Combustion*, 78:383-407
- [35] Bearman PW. 1967. The Effect of Base Bleed on the Flow Behind a Two-Dimensional Model with a Blunt Trailing Edge. *Aeronautical. Quarterly*, 18:20724
- [36] Blevins, R.D., 1985. The Effect of Sound on Vortex Shedding from Cylinders. *Journal of Fluid Mechanics* 161, 217-237
- [37] Detemple-Laake, e.; Eckelmann, H. 1989 Phenomenology of Karman Vortex Streets in Oscillatory Flow. *Experiments. in Fluids*, 7:217-227
- [38] Hsiao, F.B, Shyu, J.Y., 1991. Influence of Internal Acoustic Excitation upon Flow Passing a Circular Cylinder. *Journal of Fluids and Structures* 5:427-442
- [39] Huang X.Y., 1995. Suppression of Vortex Shedding From a Circular Cylinder by Internal Acoustic Excitation. *Journal of fluids and structures* 9:563-570
- [40] Fujisawa, N., Takeda, G., 2003. Flow Control Around a Circular Cylinder by Internal Acoustic Excitation. *Journal of Fluids and Structures* 17, 903-913.
- [41] Fujisawa, N., Takeda, G., Ike, N., 2004. Phase Averaged Characteristics of Flow Around a Circular Cylinder Under Acoustic Excitation Control. *Journal of Fluids and Structures* 19, 159-170.
- [42] Jørgensen, F.E., 2002. How to Measure Turbulence With Hot-wire Anemometers-a Practical Guide
- [43] Sreenivasan, K.R., 1981 Approach to Self Preservation in Plane Turbulent Wakes. *AIAA Journal*. 19, 1365-1367
- [44] Ramaprian, B.R., Patel, V.C., Sastry, M.S., 1982, The Symmetric Turbulent Wake of a Flat Plate. *AIAA Journal*. 20, 1228-1235
- [45] Lee, S.C., Harsha, P.T., 1970. Use of Turbulent Kinetic Energy in Free Mixing Studies. *AIAA Journal*. 8, 1026-1032

APPENDICES

APPENDIX A CALIBRATION

This appendix describes the calibration procedure for the pressure transducer and the hot wires. The calibration for both of them were carried out before each experiment.

A.1 Pressure transducer calibration:

The pressure transducer was calibrated against a known pressure from a micro manometer. The fluid used in the manometer was water. A piston arrangement was used for applying known amount of pressure. The working principle of the micrometer is same as normal manometer but the indication system is based on micrometer and conduction. When the micrometer plunger barely touches the water column, the indicator needle deflects due to conduction of current. So during pressure measurement, subsequent increase in pressure can be determined by first raising the micrometer plunger to required height and then increasing the pressure till the water column touches the micrometer plunger, again indicated by the deflection in the needle. The following steps were followed for pressure transducer calibration.

1. The carrier demodulator (always connected to the pressure transducer) was switched on.
2. The port (marked with a + sign) of the pressure transducer was connected to one of the outlet of a 'T' pipe joint
3. The other two ports were connected to the manometer and the piston respectively(piston rod at extreme end position). The water in both the arms of the manometer should be at the same level.
4. The micrometer plunger was first touched the water column then lifted up by 0.1 inch .
5. The piston was operated slowly such that the water column touched the plunger and the needle deflected to indicate there was an increment of 0.2 inch pressure in the manometer.
6. The reading in the digital display of the carrier demodulator was noted down along with the water column pressure in the manometer.
7. Step 4 was repeated upto 2 inch of water column pressure.
8. A straight line was fitted to the data. The equation of the straight line was used to compute an unknown pressure corresponding to a known voltage.

Table A.1 shows the values obtained during a typical calibration.

Voltage (V)	Pressure (inches of water)
0.78	0.2
1.54	0.4
2.23	0.6
2.94	0.8
3.71	1.0
4.46	1.2
5.22	1.4
5.95	1.6
6.71	1.8
7.36	2.0

Table A.1: Calibration chart for pressure transducer

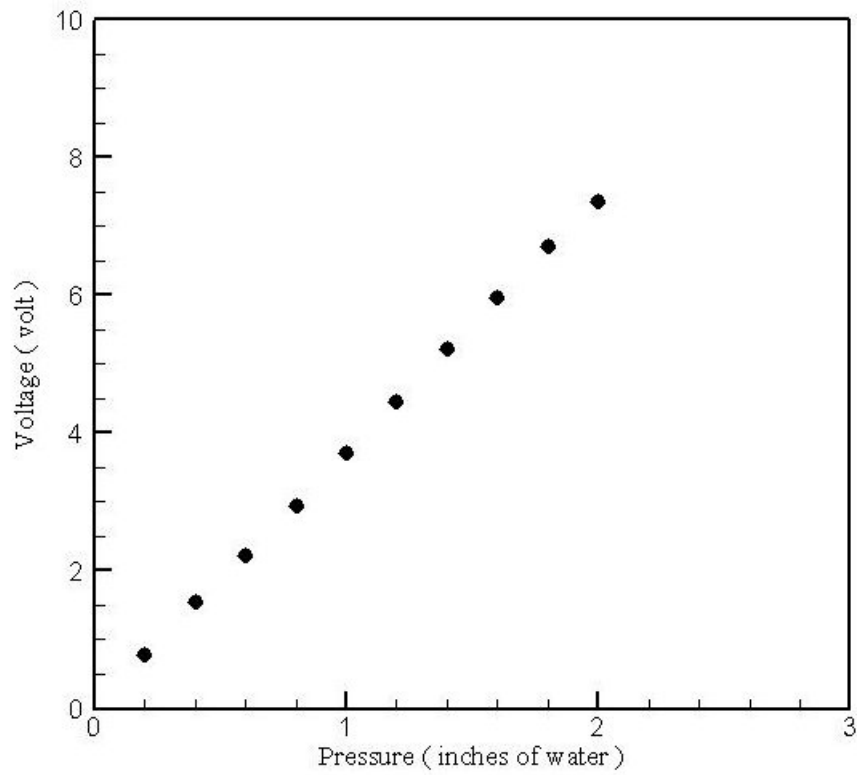


Figure A.1: Calibration curve for pressure transducer

Voltage (V)	Velocity (ft / sec)
1.79417	21.09011
1.859322	27.963432
1.913088	34.690122
1.951538	40.159858
1.993016	46.806027
2.024436	52.274944
2.050236	57.328674
2.07492	62.262415
2.091009	65.743002
2.106076	69.222534

Table A.2: Calibration chart for single wire

A.2 Calibration of the hot wire:

The hot wires were calibrated insitu in the wind tunnel. The insitu calibration was preferred to a dedicated calibrator, since the former takes care of the disturbance caused by the probe holder, the effect of geometry of the tunnel etc. The reference velocity for the calibration was found from a pitot tube placed at almost same height of the hot wire. But care was taken such that the wake of the pitot tube did not interfere with the hot wire probe. The pitot tube was connected to the Validyne pressure transducer. The tunnel velocity was increased in step from the beginning value, from the control pannel. The corresponding pressure reading was found from the display of carrier demodulator and using the pressure calibration curve it was converted to pressure in inch of H_2O . The output signal of the constant temperature anemometer was sampled at a rate of 4k Hz and a total of 12k samples were sampled. Following this procedure 12-14 data points were acquired. All these steps were implemented by a LabVIEW code. After the calibration, a transfer function which was a 4th degree polynomial, was fitted to the data. The curve fitting was carried out in MATLAB software. Table A.2 shows a typical calibration chart for a single wire. For the calibration of the x-wire, the cross wire was kept at an angle of 45° with the mean flow vector. The calibration was done in the same way as the single wire. The signal from the two wires were sampled simultaneously. Table A.3 shows a typical calibration chart for a x wire.

A.2.1 Determination of two component of velocity from X-wire:

X wires or cross wires are used to determine two velocity components of a flow field. Generally the wires are kept inclined to each other at an angle (Most of the cases it is 90°). And one of the wire faces the flow at 45° . If the plane of the two probes coincides with the x-y plane, the u and v component can be obtained from the cross wire data. The hot wire works on the principle of heat convection by the fluid flowing over the wires. The heat transfer is maximum mainly due to the velicity perpendicular to the wire (v_N). Although the velocity tangential to the wire (v_T) also contribute to the heat transfer. So the effective

$Voltage_{wire1}$ (V)	$Voltage_{wire2}$ (V)	$Velocity$ (ft / sec)
1.939586	1.687787	12.24
2.010026	1.751915	20.39
2.081031	1.8147	29.58
2.142906	1.867818	38.93
2.190952	1.909919	47.33
2.228734	1.943295	54.79
2.268396	1.978856	63.57
2.296547	2.004542	70.25
2.317002	2.022515	75.40
2.336462	2.040051	80.59
2.360009	2.062149	87.15
2.370573	2.071888	90.48

Table A.3: Calibration chart for x wire

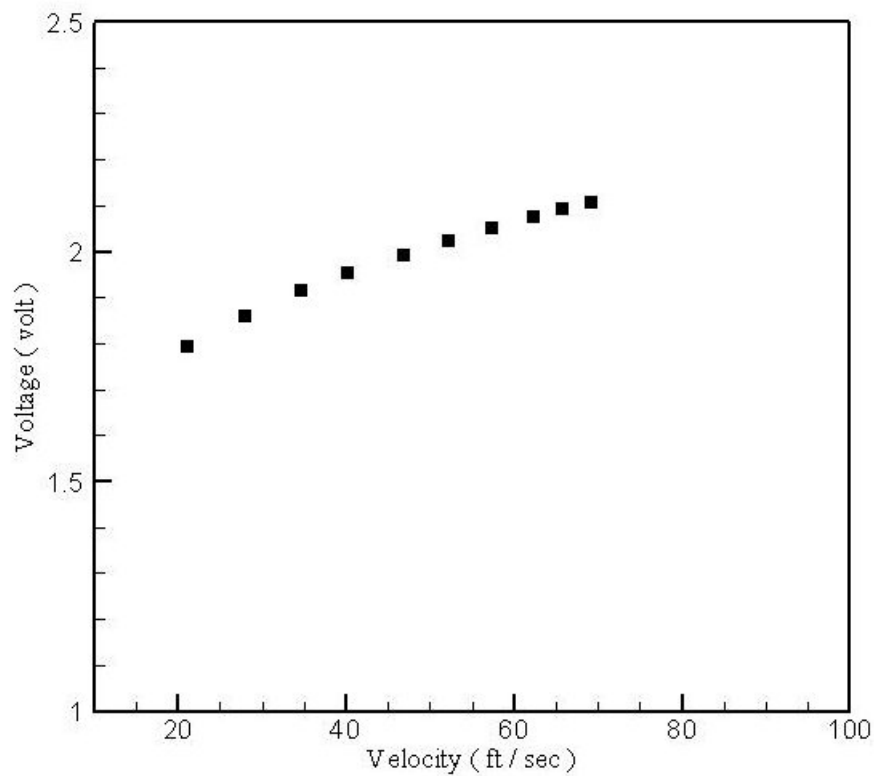


Figure A.2: Calibration curve for single wire

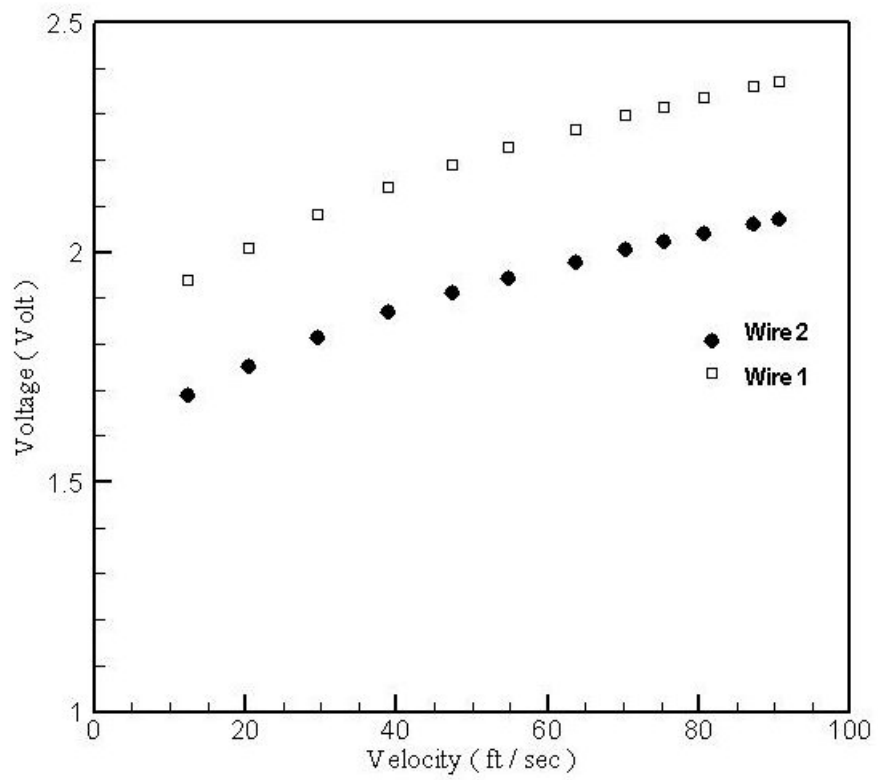


Figure A.3: Calibration curve for x wire

cooling velocity can be written as

$$v_{eff} = \sqrt{v_N^2 + k_T^2 v_T^2 + k_N^2 v_{BN}^2}; \quad (\text{A.1})$$

where v_{BN} is the velocity perpendicular to both the wire and the prongs. k_T and k_N are empirically determined constants. If the angle between the wires is 90° and one of the wire makes an angle of α° with the mean flow vector (u,say along x direction), then from [A.1] we get

$$v_{A,eff}^2 = (u \cos \alpha - v \sin \alpha)^2 + k_T^2 (u \sin \alpha + v \cos \alpha)^2 + k_N^2 w^2 \quad (\text{A.2})$$

$$v_{B,eff}^2 = (u \sin \alpha + v \cos \alpha)^2 + k_T^2 (u \cos \alpha - v \sin \alpha)^2 + k_N^2 w^2 \quad (\text{A.3})$$

where $v_N = u \cos \alpha - v \sin \alpha$ and $v_T = u \sin \alpha + v \cos \alpha$ and $w = v_{BN}$. If the sensors are sufficiently long $k_T \rightarrow 0$ and $k_N \rightarrow 1$. If the third velocity w component is small it can be neglected. Further if $\alpha = 45^\circ$

$$v_{A,eff}^2 = (u \cos \alpha - v \sin \alpha)^2 \quad (\text{A.4})$$

$$v_{B,eff}^2 = (u \sin \alpha + v \cos \alpha)^2 \quad (\text{A.5})$$

so we get

$$u = 2^{-\frac{1}{2}} (v_{A,eff} + v_{B,eff}) \quad (\text{A.6})$$

$$v = 2^{-\frac{1}{2}} (v_{A,eff} - v_{B,eff}) \quad (\text{A.7})$$

APPENDIX B
UNCERTAINTY ANALYSIS

In order to quantify the experimental uncertainties involved with a hot wire measurement, the following uncertainty calculation was carried out in accordance with the method prescribed in [42]. The reference case selected for the uncertainty evaluation was that of Reynolds number of 24,000 which corresponds to 9 m/sec. The uncertainties involved in the calculation of mean velocity profiles are addressed here. For calculation of uncertainty the following sources of error were considered (uncertainty due to temperature and pressure variation is ignored).

1. Pressure transducer error

From the data sheet provided by the manufacturer, the accuracy of pressure transducer was found to be 0.5% of full scale output.

2. Pressure transducer calibration error

The source of this uncertainty is related to curve fitting errors. A straight line was fitted to the data given in Table A.1. The residual at each data point was found out by using curve fitting toolbox in MATLAB. The residuals denote the error at each data point. The standard deviation of the errors (in % form) were calculated. The relative standard uncertainty was calculated using the formula

$$relative\ standard\ uncertainty = 2 * \frac{1}{100} standard\ deviation(errors, \%) \quad (B.1)$$

3. Hot wire calibration error

As discussed earlier, a fourth order polynomial was fitted to the data presented in Table A.2. The residuals and the corresponding relative standard uncertainty were calculated in the same way as pressure transducer calibration.

4. A/D board resolution error

The A/D board resolution error was calculated using the formula

$$relative\ standard\ uncertainty = \frac{1}{\sqrt{3}} \frac{1}{U} \frac{E_{AD}}{2^n} \frac{\partial U}{\partial E} \quad (B.2)$$

where E_{AD} is the A/D board input range, n is its resolution in bits, U the velocity and $\frac{\partial U}{\partial E}$ is the slope (sensitivity factor) of the inverse calibration curve (single wire calibration) For the A/D board used in this experiments (NI-PCI 6035E), $E_{AD} = 20v$, $\frac{\partial U}{\partial E} = 125.71$ at 30ft/sec, and $n = 16$.

<i>Errorsource</i>	<i>Value</i>	<i>Coverage factor(k)</i>	<i>Relative standard uncertainty</i>
Calibrator	0.02	2	0.01
Pressure transducer calibration	0.02	2	0.01
Hot wire calibration	0.0014	2	0.0007
A/D board resolution	0.0013	$\sqrt{3}$	0.0002

Table B.1: Uncertainties for a single velocity sample acquired with a single wire for mean velocity profile calculation

Voltage (V)	Pressure (inches of water)	residues
0.78	0.2	-0.00188
1.54	0.4	-0.0081
2.23	0.6	0.0047
2.94	0.8	0.012
3.71	1.0	0.0031
4.46	1.2	-0.00039
5.22	1.4	-0.0066
5.95	1.6	-0.004679
6.71	1.8	-0.01089
7.36	2.0	0.01274

Table B.2: Calibration chart for pressure transducer with residues

B.1 Velocity sample uncertainty:

The relative uncertainties are presented in Table B.1.

So the total uncertainties involved is $2\sqrt{0.01^2 + 0.01^2 + 0.0007^2 + 0.0002^2} = 0.0283 = 2.83\%$

B.2 Sample calculation of pressure transducer calibration uncertainty:

In this section a sample calculation of the uncertainties is presented whose source is the curve fitting errors. Table A.1 is again presented here as B.2 with an extra column which contains the residues (errors due to the fitting of a straight line to the data).

As mentioned earlier MATLAB's cfit toolbox was utilised for this computation. It stored the residues in a structure output1.residue and the pressure values were stored in a variable y. The following MATLAB code was executed to get the relative standard uncertainty (rsu) due to pressure transducer calibration. $rsu = 2 * std(100 * output1.residue./y)/100$ which gives 0.02 as result.